



UvA-DARE (Digital Academic Repository)

Organic carbon cycling in a Caribbean coral reef

Hidden biomass, sneezing sponges, and net heterotrophy

Kornder, N.A.

Publication date

2023

[Link to publication](#)

Citation for published version (APA):

Kornder, N. A. (2023). *Organic carbon cycling in a Caribbean coral reef: Hidden biomass, sneezing sponges, and net heterotrophy*. [Thesis, fully internal, Universiteit van Amsterdam].

General rights

It is not permitted to download or to forward/distribute the text or part of it without the consent of the author(s) and/or copyright holder(s), other than for strictly personal, individual use, unless the work is under an open content license (like Creative Commons).

Disclaimer/Complaints regulations

If you believe that digital publication of certain material infringes any of your rights or (privacy) interests, please let the Library know, stating your reasons. In case of a legitimate complaint, the Library will make the material inaccessible and/or remove it from the website. Please Ask the Library: <https://uba.uva.nl/en/contact>, or a letter to: Library of the University of Amsterdam, Secretariat, P.O. Box 19185, 1000 GD Amsterdam, The Netherlands. You will be contacted as soon as possible.



Chapter

2

Implications of 2D versus 3D surveys to measure the abundance and composition of benthic coral reef communities

Niklas A Kornder, Jose Cappelletto, Benjamin Mueller, Margaretha J L Zalm, Stephanie J Martinez, Mark J A Vermeij, Jef Huisman & Jasper M de Goeij

Published in *Coral Reefs*, 40(4), 1137–1153 (2021)

ABSTRACT

A paramount challenge in coral reef ecology is to estimate the abundance and composition of the communities residing in such complex ecosystems. Traditional 2D projected surface cover estimates neglect the 3D structure of reefs and reef organisms, overlook communities residing in cryptic reef habitats (e.g., overhangs, cavities), and thus may fail to represent biomass estimates needed to assess trophic ecology and reef function. Here, we surveyed the 3D surface cover, biovolume, and biomass (i.e., ash-free dry weight) of all major benthic taxa on 12 coral reef stations on the island of Curaçao (Southern Caribbean) using structure-from-motion photogrammetry, coral point counts, *in situ* measurements, and elemental analysis. We then compared our 3D benthic community estimates to corresponding estimates of traditional 2D projected surface cover to explore the differences in benthic community composition using different metrics. Overall, 2D cover was dominated ($52 \pm 2\%$, mean \pm SE) by non-calcifying phototrophs (macroalgae, turf algae, benthic cyanobacterial mats), but their contribution to total reef biomass was minor ($2.8 \pm 0.5\%$). In contrast, coral cover ($32 \pm 2\%$) more closely resembled coral biomass ($27 \pm 6\%$). The relative contribution of erect organisms, such as gorgonians and massive sponges, to 2D cover was 2- and 11-fold lower, respectively, than their contribution to reef biomass. Cryptic surface area ($3.3 \pm 0.2 \text{ m}^2 \text{ m}^{-2}_{\text{planar reef}}$) comprised half of the total reef substrate, rendering two thirds of coralline algae and almost all encrusting sponges (99.8 %) undetected in traditional assessments. Yet, encrusting sponges dominated reef biomass ($35 \pm 18\%$). Based on our quantification of exposed and cryptic reef communities using different metrics, we suggest adjustments to current monitoring approaches, and highlight ramifications for evaluating the ecological contributions of different taxa to overall reef function. To this end, our metric conversions can complement other benthic assessments to generate non-invasive estimates of the biovolume, biomass, and elemental composition (i.e., standing stocks of organic carbon and nitrogen) of Caribbean coral reef communities.

INTRODUCTION

Ecological models offer insights into complex community dynamics and biogeochemical cycling within ecosystems, but depend on accurate abundance estimates (i.e., composition and biomass) of taxa comprising communities (Diaz and Rützler 2001; van Oevelen et al. 2006). In coral reef ecology, the abundance of organisms is traditionally assessed as the percentage of the projected reef substrate covered by each organismal group (Kohler and Gill 2006; Sandin et al. 2008a). While this two-dimensional (2D) approach can be useful to produce relatively fast estimates of the “health” of a reef ecosystem (e.g., coral or macroalgal cover), it ignores the complex, three-dimensional (3D) morphology of coral reefs and the reef organisms themselves (Goatley and Bellwood 2011). Planar, projected images ignore differences in volume and biomass of erect versus non-erect organisms (e.g., gorgonians versus crustose coralline algae) and do not capture the abundance and composition of hidden benthic taxa occurring in the cryptic reef habitat (e.g., holes, overhangs, crevices, cavities), also referred to as ‘coelobites’ (Choi 1982). A lack of reef-wide biomass assessments that adequately incorporate habitat complexity and cryptic habitats could therefore potentially limit our understanding of how coral reef ecosystems function at present and develop in the future.

The critical role of habitat complexity in maintaining high biodiversity and community abundance within benthic ecosystems is well-established (Kostylev et al. 2005; Kovalenko et al. 2012; Tokeshi and Arakaki 2012). To assess this complexity, numerous studies recently applied structure-from-motion photogrammetry—a technique in which 3D models are generated from a stack of images depicting objects from various angles—to estimate parameters describing the 3D topographic structure of either reef surfaces (Burns et al. 2015; Leon et al. 2015; Ferrari et al. 2016; Storlazzi et al. 2016) or individual reef organisms (Figueira et al. 2015; Lavy et al. 2015; Gutierrez-Heredia et al. 2016). Structural parameters of reef surfaces and organisms were shown to be estimated with relatively high accuracy using photogrammetry in combination with underwater action cameras (Veal et al. 2010; Guo et al. 2016; but see Bryson et al. 2017) that would be small enough to access and photograph cryptic reef surfaces. While these parameters were used, for example, to better explain variation in the occurrence of mobile fish populations (Gratwicke and Speight 2005; Harborne et al. 2012), attempts to implement photogrammetry to assess the overall abundance and composition of benthic reef communities, including cryptic habitats, are so far lacking.

Cryptic habitats are estimated to account for 75–90 % of the volume of a coral reef ecosystem (Choi and Ginsburg 1983; Ginsburg 1983) and up to 8 m² of additional substrate can be found underneath each projected m² of reef surface

2 (Richter et al. 2001; Scheffers et al. 2004). Cryptic substrates are generally densely populated by a distinct benthic community comprised of crustose coralline algae (CCA), encrusting sponges, bryozoans, tunicates and polychaetes (e.g., Winston and Jackson 1984; Wunsch et al. 2000; Scheffers et al. 2004; van Duyl et al. 2006). To the best of our knowledge, there is only a single assessment of cryptic surface areas (Richter and Wunsch 1999; Richter et al. 2001) combined with associated coelobite community sizes (Wunsch et al. 2000) from one geographic region (Northern Red Sea) conducted two decades ago. These seminal studies were limited to accessible cavities, ignoring communities in smaller cryptic spaces, such as the undersides of plating corals (Jackson and Winston 1982). Further, they lack biomass estimates of constituent species needed to study functional interactions between cryptic and exposed reef communities, essentially rendering cryptic spaces the ‘largest, but least known habitat on coral reefs’ (de Goeij and van Duyl 2007). Cryptic habitats act as major sinks of particulate (Richter and Wunsch 1999) and, predominantly, dissolved organic matter (de Goeij and van Duyl 2007), and can provide a source of inorganic nutrients that sustain productivity of nearby cryptic and exposed reef organisms (Rasheed et al. 2002; Scheffers et al. 2004; de Goeij et al. 2013), increasing the diversity of reef communities as a whole (Slattery et al. 2013). Comprehensive data on the composition of the entire benthic reef community, including cryptic habitats, are therefore needed to better understand the functional dynamics on coral reefs (Chapin et al. 1997; McCauley et al. 2018).

At present, we do not know to what extent 2D-projections of 3D organisms and the exclusion of cryptic communities in benthic reef surveys influence estimates of the relative abundances and biomass distributions of benthic reef organisms. Therefore, we created an overall census of all major sessile benthic taxa (i.e., scleractinian corals, gorgonians, calcifying algae, non-calcifying phototrophs, massive, and encrusting sponges) in both exposed and cryptic habitats along the leeward fringing reef on the Caribbean island of Curaçao. First, we determined exposed and cryptic surface areas per m² of projected reef by 3D reconstruction. Secondly, we assessed the relative cover of each benthic group using common 2D benthic surveys on horizontal, but also vertical and cryptic reef surfaces. Thirdly, we measured the biovolume of all erect taxa directly *in situ*. Finally, we produced metric conversion factors for 53 resident species to estimate the biomass of all major sessile benthic groups. This approach enabled us to explore the differences in benthic community composition derived from 2D and 3D benthos surveys. Since different benthic groups perform different ecological functions (e.g., primary and secondary production, calcification, etc.), we aimed to determine a baseline for the benthos on the leeward reef slopes of Curaçao, with potential implications for our overall understanding of the ecosystem functioning of coral reefs.

METHODS

General survey design and sampling approach

All assessments of benthic communities in both cryptic and exposed reef habitats were conducted from March to June 2018 at 12 reef sites along the leeward shore of Curaçao (Figure S1, Online resource 1). Sites were chosen to cover a representative range of reef types (healthy vs. degraded, flat vs. complex) along the southwest coast of Curaçao (WAITT-Institute 2017). Based on our sampling design, each site was defined as a 120 m long stretch of reef slope between 9–14 m water depth. At each of the 12 sites, two 40-m transects (with 40 m distance between them) were laid out parallel to shore. Measurements and imaging (see below) were conducted in 16 quadrats per site (15 for site Jeremi), spaced apart at 4-m intervals on alternating sides of the two transects. Each quadrat represents all exposed and cryptic reef surfaces within a planar, projected reef area of 1 by 1 m, and was confined by positioning a frame made of PVC pipes. For each quadrat, the water depth and structural relief (i.e., the distance between the lowest and highest point of the reef in contact with the surrounding water) was measured using an Oceanic Veo 3.0 dive computer (0.1 m accuracy). Additional measurements in each quadrat, described in more detail further below, included:

- 3D reconstructions of cryptic and exposed reef surface areas (in $\text{m}^2 \text{m}^{-2}_{\text{planar reef}}$),
- additional surface area measurements of cryptic surfaces not detected in 3D reconstructions,
- relative cover (in % of total benthos) of the benthic groups occurring on exposed horizontal and vertical, and cryptic reef surfaces,
- volumes of all erect organisms (gorgonians and massive sponges) (in $\text{dm}^3 \text{m}^{-2}_{\text{planar reef}}$),
- canopy heights of non-calcifying phototrophs on exposed horizontal and vertical, and cryptic surfaces.

Additional measurements included tissue thicknesses (in cm) of 30 species and various biomass measures (in g cm^{-2} or g cm^{-3}) of 53 species (Online resource 2). All measures were combined to estimate site specific ($n = 16$ quadrats per site, except Jeremi where $n = 15$) and island-wide ($n = 191$ quadrats in total) relative abundances of benthic reef organisms in terms of 3D surface area, biovolume, and biomass.

Surface area estimation of exposed and cryptic habitats

Total reef surface areas within each quadrat were obtained from 3D reconstructions of the reef surface. Our estimates of reef surface area (in $\text{m}^2 \text{m}^{-2}_{\text{planar reef}}$) can be interpreted as measurements of reef rugosity in 3D, although

scale differences need to be considered when comparing rugosities determined by different methods. The 3D reconstructions were based on 200–350 overlapping (> 60 %) images of all photographable surfaces within each quadrat—excluding small cryptic crevices or deep holes, which were quantified *in situ* (see below)—using a GoPro HERO6 Black camera (settings: resolution: 4000 x 3000 pixels; aperture: f/2,8; exposure 1/60 second, ISO gain and white balance: automatic) and three GoBe 800-lumen video lights to improve uniform illumination of all visible surfaces. We applied a structure-from-motion method for image acquisition and 3D-model generation that was previously established for structural complexity and surface analysis of coral reef 3D reconstructions (Burns and Delparte 2017; Young et al. 2018; Bayley et al. 2019). The 1 x 1 m PVC frames were removed during image acquisition after placing four 15-mL sand-filled Falcon tubes at the corners of each quadrat. Two spirit levels were placed horizontally at a 90° angle on a tripod next to each quadrat to accurately define a horizontal reference plane for the angles of all surface elements in our 3D reconstructions. In addition, the known lengths of the Falcon tubes and spirit levels served as scale bars for the 3D reconstructions.

To generate a 3D representation of all surfaces within each quadrat, (1) images were resized to 2500 x 1875 pixels using the Lanczos resampling algorithm, (2) color adjusted to compensate for site-specific differences in lighting, and (3) an automatic contrast enhancement step was added to facilitate detection and identification of organisms and reef structures. All pre-processing of images was done in XNConvert (<https://www.xnview.com/en/xnconvert/>). Pre-processed images were exported as JPEG files at maximum compression quality and uploaded in Agisoft Photoscan (Version 1.4; Agisoft, St. Petersburg, Russia; <http://www.agisoft.com/downloads/>). This program was used to create 3D representations of all visible surfaces in reef quadrats using the following configurations: (1) align photos: generic image pre-selection, 20,000 key point limit and 8,000 tie point limit, (2) dense reconstruction: mild depth filtering, medium density, (3) mesh reconstruction: arbitrary 3D surface, 450,000 faces and (4) build texture: generic mapping mode, mosaic blend, single texture (4096 x 1). The *marker and rule* tools in Photoscan were used to calibrate all 3D models using the Falcon tubes and the spirit levels for scale. Models were aligned horizontally in reference to the spirit levels and cropped to a 1 by 1 m planar footprint (i.e., 1 quadrat) using the rectangular cropping tool in Photoscan and the four Falcon tubes as reference points. Finally, quadrat models (accuracy: 0.323 ± 0.164 cm, mean \pm SD) were saved as Wavefront OBJ files and imported into MeshLab (Cignoni et al. 2008) for surface post-processing and size measurements.

From each 3D quadrat model, information for each surface element, including surface area, angle, and an estimate of exposure to external observers (i.e., to

annotate surface elements to being either cryptic or exposed; see below), was extracted in MeshLab. First, 3D quadrat models were resampled by applying a clustering decimation filter using a cell size of 5 mm to ensure resolution consistency across all reconstructions, after which a two-step Gaussian smoothing filter was applied to remove noise (i.e., spurious 3D points from suspended particles or moving objects). Filter parameters used were: (1) directional bias: 0.5, (2) requested views: 128, (3) lightning direction: [0, 0, 1] (Nadir pointing Sunlight source) and (4) cone amplitude: 60 degrees. Second, the angle (θ) of each mesh element toward the water surface was computed as the perpendicular vectors of the element (e.g., $\theta = 0^\circ$ indicates a plane parallel to the water surface). Third, each element's exposure to external observers was estimated based on an ambient occlusion algorithm (Landis 2002; Sabbadin et al. 2016, Supplementary text 1), which is a commonly applied method for 3D models in computer graphics and animations. This algorithm estimates an exposure index for each surface point. The exposure index is defined as the percentage of a full 180 degrees field of view from the surface point that is not occluded by any obstacles, i.e., that is in a direct line of sight with external observers looking at the reef's surface (see the drawing in Figure S2). Thus, an exposure index of 30% implies that the surface point is visible for 30% of all possible sight lines across a 180 degrees field of view, while it is hidden behind obstacles for the remaining 70%. We used the exposure index to categorize modeled reef surfaces as being either cryptic (hidden) or non-cryptic (exposed). For this purpose, we first applied the ambient occlusion algorithm to all surface elements in 3D models of three known exposed (i.e., flat reef tops) and three known cryptic (i.e., cavities) reef surfaces, generating frequency distributions of exposure indices for each of the two surface types (Figure S3). The frequency distributions of these known exposed and cryptic reef surfaces intersected at an exposure index of 17.5%. Therefore, we choose an exposure index of 17.5% as our threshold value to distinguish between exposed and cryptic surfaces. This implies that cryptic surfaces are “out of sight” for at least 82.5% of all possible sight lines within a 180 degrees field of view.

Exposed surfaces were further distinguished into rather horizontal ($0^\circ < \theta < 45^\circ$) and rather vertical ($45^\circ \leq \theta < 135^\circ$) surfaces to account for the fact that communities on these substrates differ (Duran et al. 2018). After analysis, all metrics for exposed horizontal and vertical surfaces were merged to obtain combined estimates of surface areas, volumes, and biomasses for each benthic group on exposed surfaces.

To estimate the total surface area of horizontal and vertical exposed and cryptic reef surfaces, txt files with each element's surface area, angle, and light index were exported from MeshLab, sorted by surface type and summed in R (R Development

Core Team 2010). Example illustrations of the individual processing steps to generate 3D reconstructions of each quadrat are provided in Figure S4.

Small crevices and deep holes inaccessible for our camera did not appear in the photogrammetric 3D reconstructions, so their surfaces and volumes (Online resource 3) were measured by hand *in situ* and approximated based on formulas of closest known geometrical shapes (i.e., sphere, cylinder, etc.). To account for the lack of fine-scale substrate rugosity associated with geometrical approximations, the ratio of image-based area over hand-measured area was calculated in three accessible caves. The average ratio (1.34 ± 0.10 ; \pm SE) was then used to correct for the underestimation of surfaces from geometric-based cave measurements compared to photogrammetric 3D reconstructions. To quantify cryptic surfaces existing on the underside of sheeting (e.g., *Agaricia* spp.) or at the base of stalking corals (e.g., *Eusmilia fastigiata*, *Madracis mirabilis*), these corals were photographed from several angles ($n = 13$ for *Agaricia* spp. and $n = 18$ for stalking corals). The images were scaled in ImageJ (version 1.X) (Schneider et al. 2012) to estimate surface areas of live coral and cryptic substrate using the *framing tool*. The ratio of cryptic substrate area to live coral area yields the proportional cryptic surface at the undersides of sheeting corals (57 ± 4 % of live sheeting coral surface) and bases of stalking corals (231 ± 26 % of live stalking coral surface, Online resource 4), which we then applied to our 3D surface area estimates for these corals to calculate the cryptic surface underneath these corals. Total cryptic surface area was estimated by adding these additional cryptic surfaces to our 3D reconstructed cryptic surfaces. Since smaller and highly inaccessible cavities and crevices could not be accessed, we acknowledge that our estimates of cryptic surface areas must be considered underestimations and are therefore conservative.

Relative cover on exposed and cryptic reef surfaces

Based on their taxonomic identity and morphological growth form, the sessile benthic species were classified into gorgonians, massive corals, branching corals, encrusting corals, foliose corals, sheeting corals, stalking corals, solitary corals, massive sponges, encrusting sponges, CCA, *Peyssonnelia* spp., *Halimeda* spp., macroalgae, turf algae, benthic cyanobacterial mats, bivalves, tunicates, polychaetes, hydrozoans, and bryozoans (see Tables S1 and S2 for individual species and group allocations; see Online resource 5 for raw cover data). Sponges were identified to the lowest taxonomic level possible based on photographs and field surveys. The species were further aggregated into 7 major benthic groups: gorgonians, scleractinian corals, massive sponges, encrusting sponges, calcifying algae, non-calcifying phototrophs, and others (Table 1).

The percentage of surface covered by the different benthic groups was quantified for horizontal and vertical exposed and cryptic surfaces separately, in

each of the 191 quadrats. A Nikon Coolpix P7000 (Nikon Corp., Japan) underwater camera was used to first obtain one 1 m² top-view image of each quadrat as in traditional reef surveys (horizontal cover; n = 16 images per site). An INON S-2000 strobe (INON Inc., Japan) was used to ensure proper lighting and avoid shadows. Subsequently, for each quadrat, three side-view images of haphazardly determined vertical reef surfaces were made with the same camera equipment to estimate vertical cover (n = 48 images per site, with an average surface area of 450 ± 280 cm² (mean ± SD) per image). Whenever possible, we chose one surface parallel to the reef slope, and two surfaces perpendicular to the reef slope: one up- and one down-current to the long-term mean current from SE to NW. Lastly, three cryptic surfaces per quadrat were photographed using an Olympus Tough TG-5 underwater compact camera (Olympus Corp., Japan) to estimate cryptic cover (n = 48 images per site, with an average surface area of 118 ± 82 cm² per image). Specifically, for these cryptic surfaces we chose, where possible due to space limitations, one “roof” surface, one “side” surface and one “back” surface per quadrat.

Benthic community composition in each image was analyzed using point-count analyses (80 stratified random points per picture) in Coral Point Count with Excel extension (CPCe) (Kohler and Gill 2006). Some substrates were covered by communities through which the community on the underlying substrate could still be seen (e.g., turf algae with an understory of CCA). In those cases, only the overlying turf algae was counted in 2D cover estimates, while for all 3D estimates (see below), the percentage bottom cover of both overlying and underlying communities was estimated separately so that total cover estimates exceeded 100 % in some cases (see Online resource 5).

3D surface area of benthic groups

The 3D surface area of each benthic group per site (SA_i for benthic group *i*) was first calculated for horizontal and vertical exposed and cryptic surfaces separately. Average substrate surface areas (A, in m² m⁻²_{planar reef}) obtained from the 3D reconstruction of the reef were multiplied by the average relative 2D cover (C_i) of a benthic group across all 16 quadrats (or 15 for site Jeremi) per site. For example, the 3D surface area of benthic group *i* on horizontal surfaces (denoted by the subscript *ho*) was calculated as:

$$(1) \quad SA_{ho,i} = A_{ho} \cdot C_{ho,i}$$

Standard errors of these estimates were calculated by propagating standard errors of A and C (shown again for horizontal 3D surface area of benthic group *i*):

$$(2) \quad \delta SA_{ho,i} = SA_{ho,i} \cdot \sqrt{\left(\frac{\delta A_{ho,i}}{A_{ho,i}}\right)^2 + \left(\frac{\delta C_{ho,i}}{C_{ho,i}}\right)^2},$$

where δ refers to standard error (SE). Estimates for horizontal and vertical exposed and cryptic surfaces were summed up to obtain total 3D surface area per site for benthic group i (TSA, in $\text{m}^2 \text{m}^{-2}_{\text{planar reef}}$, Online resource 6). The standard error of the total surface area was obtained by propagating the standard errors from Equation (2) according to:

$$(3) \quad \delta\text{TSA}_i = \sqrt{(\delta\text{SA}_{\text{ho},i})^2 + (\delta\text{SA}_{\text{ve},i})^2 + (\delta\text{SA}_{\text{cr},i})^2},$$

where the subscripts *ve* and *cr* denote vertical and cryptic surfaces. In a similar calculation, the total exposed 3D surface area was calculated using only the values for horizontal and vertical reef surfaces. Island-wide 3D surface areas for each benthic group (e.g., group i) were calculated using the average surface areas and 2D surface cover across all 12 sites ($n = 191$ quadrats).

Biovolumes of benthic groups

Biovolumes of erect organisms (i.e., massive sponges and gorgonians) were estimated by dividing each individual into one or more geometrical forms (i.e., rods, cone, sphere, bowls, barrels, see Table S3) that were measured *in situ* using a measuring tape or ruler, taking into account accessible empty space (e.g., larger oscula of some sponges). This was done because individuals assigned to these groups often moved (in the current) and as a consequence could not be reconstructed in 3D through structure-from-motion techniques. To ensure that all erect organisms were measured in a similar manner, we also hand measured individuals that did not move in the current. The cuboid geometrical form was used to estimate the biovolume of all non-erect organisms by multiplying their 3D surface area to their average thickness. The thickness of organic tissues for each non-erect species was derived from side view photographs of broken colonies in ImageJ. Since we considered all calcified framework as substrate (including the 3D structures produced by scleractinian corals), the coral tissue itself represents a thin layer overlying such structures (Edmunds and Gates 2002) and was primarily measured as a surface rather than a volume. The biovolume of non-erect organisms can be estimated by multiplying 3D surface cover to an average tissue height of the respective organism (hence cuboid form). In contrast, erect organisms (e.g., massive sponges, gorgonians) form an individual volume (3D shape) extending from the substrate. An exception from this are non-calcifying phototrophs (i.e., turf algae, macroalgae, and benthic cyanobacterial mats), where canopy heights can vary dramatically and were therefore measured *in situ* in all quadrats for horizontal and vertical exposed and cryptic surfaces separately ($n = 3$ for each taxon per surface type per quadrat). To calculate biovolumes of turf algae and benthic cyanobacterial mats, average canopy height was multiplied by their average 3D surface area. The estimated volumes of tissue on each surface type

Abundance and composition of benthic coral reef communities

Table 1. Total abundances of benthic reef residents in terms of 2D relative cover, 3D surface area, biovolume, biomass (ash-free dry weight), and organic carbon per m² of planar reef, summed over both exposed and cryptic surfaces. Values are mean ± SE. See Tables S1, S2 and Methods for sample sizes of underlying measurements. n.d., no data.

organism	2D cover [%]	3D surface area [dm ² m ⁻² _{planar reef}]	tissue volume [dm ³ m ⁻² _{planar reef}]	ash-free dry weight [g per m ² _{planar reef}]	organic carbon [g per m ² _{planar reef}]
gorgonians	2.72 ± 0.34	5.49 ± 2.32	0.94 ± 0.14	106 ± 33.8	47.9 ± 16.0
massive sponges	1.52 ± 0.29	4.36 ± 1.80	3.53 ± 1.24	284 ± 102	126 ± 45.2
HMA sponges	1.18 ± 0.26	2.21 ± 1.55	2.65 ± 1.21	261 ± 121	116 ± 54.1
LMA sponges	0.11 ± 0.04	1.60 ± 0.89	0.30 ± 0.23	10.7 ± 8.29	4.83 ± 3.75
<i>Agelas clathrodes</i>	0.52 ± 0.16	0.82 ± 0.96	0.64 ± 0.25	61.8 ± 27.7	28.5 ± 12.6
<i>Agelas conifera</i>	0.02 ± 0.01	0.14 ± 0.22	0.02 ± 0.02	1.24 ± 1.24	0.55 ± 0.55
<i>Agelas sventres</i>	0	0.11 ± 0.15	0	n.d.	n.d.
<i>Aiolochoiria crassa</i>	0.04 ± 0.02	0.04 ± 0.03	0.17 ± 0.11	37.8 ± 25.1	17.4 ± 11.6
<i>Aplysina archeri</i>	0.07 ± 0.04	0.07 ± 0.04	0.12 ± 0.09	12.9 ± 10.1	6.01 ± 4.70
<i>Aplysina cauliformis</i>	0.02 ± 0.02	0.06 ± 0.11	0.01 ± 0.01	1.77 ± 1.77	0.82 ± 0.82
<i>Aplysina lacunosa</i>	0.16 ± 0.09	0.17 ± 0.10	0.19 ± 0.13	22.1 ± 16.0	9.81 ± 7.12
<i>Biemna sp.</i>	0	0.01 ± 0.01	< 0.005	0.02 ± 0.02	0.01 ± 0.01
<i>Callyspongia plicifera</i>	0.02 ± 0.01	0.08 ± 0.13	< 0.005	0.04 ± 0.02	0.02 ± 0.01
<i>Callyspongia vaginalis</i>	0.03 ± 0.02	0.08 ± 0.11	0.01 ± 0.01	0.56 ± 0.33	0.27 ± 0.16
<i>Desmapsamma anchorata</i>	0.01 ± 0.01	0.01 ± 0.01	0.01 ± 0.01	0.55 ± 0.54	0.24 ± 0.23
<i>Ectyoplasia ferox</i>	0	0	< 0.005	0.06 ± 0.06	0.03 ± 0.03
<i>Ircinia campana</i>	0.11 ± 0.05	0.16 ± 0.15	0.12 ± 0.07	12.2 ± 6.98	5.29 ± 3.02
<i>Ircinia felix</i>	0.10 ± 0.09	0.39 ± 0.63	0.02 ± 0.01	1.17 ± 0.64	0.45 ± 0.24
<i>Ircinia strobilina</i>	0.04 ± 0.02	0.13 ± 0.11	0.10 ± 0.04	5.29 ± 2.11	2.11 ± 0.81
<i>Neofibularia nolitangere</i>	0.07 ± 0.07	0.16 ± 0.22	0.07 ± 0.05	3.65 ± 2.50	1.53 ± 1.05
<i>Niphates erecta</i>	0.05 ± 0.02	1.42 ± 0.95	0.28 ± 0.23	12.9 ± 10.9	5.70 ± 4.82
<i>Xestospongia muta</i>	0.15 ± 0.15	0.16 ± 0.16	1.17 ± 1.17	43.1 ± 43.3	17.2 ± 17.3
Other massive sponges	0.12 ± 0.06	0.35 ± 0.38	0.23 ± 0.10	18.4 ± 8.32	8.14 ± 3.68
scleractinian corals	32.1 ± 1.58	75.3 ± 12.8	1.09 ± 0.25	456 ± 95.8	138 ± 31.0
massive corals	12.4 ± 0.93	28.3 ± 21.0	0.38 ± 0.30	245 ± 186	78.3 ± 60.1
branching corals	1.22 ± 0.18	2.91 ± 1.12	0.05 ± 0.03	12.0 ± 6.14	1.85 ± 0.89
encrusting corals	1.80 ± 0.19	12.2 ± 3.53	0.17 ± 0.07	66.2 ± 29.8	23.5 ± 10.3
foliose corals	4.28 ± 0.49	8.99 ± 1.93	0.07 ± 0.05	13.5 ± 3.27	1.72 ± 0.43
sheeting corals	1.29 ± 0.19	3.72 ± 2.26	0.05 ± 0.04	27.6 ± 18.6	10.2 ± 6.79
stalking corals	11.1 ± 1.34	18.0 ± 11.5	0.33 ± 0.25	149 ± 97.6	30.1 ± 19.9
solitary corals	0	1.13 ± 0.27	0.02 ± 0.01	6.26 ± 1.63	2.77 ± 0.78
encrusting sponges	0.07 ± 0.03	139 ± 57.3	5.30 ± 2.47	590 ± 299	271 ± 138
<i>Clathria sp.</i>	0	0.60 ± 0.42	0.01 ± 0.00	0.39 ± 0.28	0.18 ± 0.13
<i>Halisarca caerulea</i>	0	1.81 ± 1.94	0.02 ± 0.02	1.29 ± 1.40	0.57 ± 0.62
<i>Monanchora arbuscula</i>	0	0.99 ± 0.54	0.01 ± 0.00	0.68 ± 0.37	0.30 ± 0.16
<i>Phorbis amaranthus</i>	0	0.71 ± 0.57	0.03 ± 0.02	1.82 ± 1.51	0.91 ± 0.75
<i>Plakortis sp.</i>	0	0.40 ± 0.50	0.04 ± 0.06	6.23 ± 7.72	2.88 ± 3.57
<i>Scopalina ruetzleri</i>	0.05 ± 0.02	4.49 ± 2.03	0.21 ± 0.10	18.1 ± 8.86	7.73 ± 3.80
other encrusting sponges	0.02 ± 0.02	130 ± 131	4.96 ± 5.13	552 ± 571	253 ± 262

2

organism	2D cover [%]	3D surface area [dm ² m ⁻² planar reef]	tissue volume [dm ³ m ⁻² planar reef]	ash-free dry weight [g per m ² planar reef]	organic carbon [g per m ² planar reef]
excavating sponges	0.31 ± 0.09	1.67 ± 0.85	n.d.	n.d.	n.d.
<i>Cliona spp.</i>	0.15 ± 0.08	0.38 ± 0.35	n.d.	n.d.	n.d.
<i>Siphonodictyon spp.</i>	0	0.85 ± 0.18	n.d.	n.d.	n.d.
other excavating sponges	0.16 ± 0.05	0.43 ± 0.34	n.d.	n.d.	n.d.
non-calcifying phototrophs	51.6 ± 1.57	176 ± 33.9	3.21 ± 0.32	46.3 ± 8.20	21.0 ± 3.90
benthic cyanobacteria	3.20 ± 0.31	7.44 ± 3.25	0.55 ± 0.24	0.19 ± 0.10	0.12 ± 0.06
macroalgae	29.1 ± 1.55	96.8 ± 21.2	0.10 ± 0.02	36.8 ± 8.06	17.5 ± 3.84
turf algae	19.4 ± 1.17	71.9 ± 5.29	2.55 ± 0.20	9.27 ± 1.49	3.36 ± 0.69
calcifying algae	2.99 ± 0.37	129 ± 19.0	0.61 ± 0.21	151 ± 32.1	43.6 ± 11.3
crustose coralline algae	1.68 ± 0.29	70.1 ± 13.0	0.18 ± 0.03	90.7 ± 22.9	15.7 ± 3.42
<i>Halimeda sp.</i>	1.03 ± 0.22	2.98 ± 1.90	0.01 ± 0.01	1.67 ± 1.09	0.55 ± 0.36
<i>Peyssonellia spp.</i>	0.28 ± 0.06	56.6 ± 14.5	0.52 ± 0.13	90.9 ± 28.4	36.0 ± 11.0
other	8.59 ± 0.71	10.6 ± 0.81	1.34 ± 0.41	49.4 ± 11.8	21.8 ± 6.65
bryozoans	0	1.85 ± 0.23	n.d.	n.d.	n.d.
hydrozoans	0	22.6 ± 1.44	0.67 ± 0.40	31.4 ± 11.6	17.2 ± 6.63
<i>Lithophaga sp.</i>	0	8.71 ± 0.73	0.37 ± 0.07	12.5 ± 1.33	2.70 ± 0.28
polychaetes	0.44 ± 0.10	15.7 ± 3.74	n.d.	n.d.	n.d.
<i>Didemnum sp.</i>	0	9.53 ± 0.79	0.27 ± 0.04	3.68 ± 0.35	1.10 ± 0.25

were then summed and their errors propagated analogous to Equation (3) to calculate overall biovolume in dm³ m⁻²planar reef.

The dominant macroalgae (*Dictyota spp.* and *Lobophora spp.*) were difficult to discern on CPCe images and therefore assessed as a single benthic group. Further, these algae grow in loose bundles of leaves that can be more or less dense. This means the empirical relationships between canopy height and tissue volume for a given surface area may not be linear, rendering the cuboid calculation potentially erroneous. We therefore first calculated the empirical regression between canopy height and tissue volume for a total of 9 tissue samples of each species covering 25–160 cm² of substrate with varying canopy height (Figure S5A,B, Table S4). For each sample, thallus surface area was estimated by laying out all thalli on a white sheet and taking scaled images to be analyzed for total surface area in ImageJ. The tissue volume of these samples was calculated by multiplying thallus surface area with average thallus thicknesses of 70 μm for *Dictyota* and 40 μm for *Lobophora*, respectively (Tronholm et al. 2010; Vieira 2015; Camacho et al. 2019), and then regressed against the sampling area. The average *in situ* canopy height of macroalgae was inserted (x-value) into these empirical regressions to calculate conversion factors (i.e., y-values in Figure S5A,B) from 3D surface area to volume for that quadrat and surface type (see Supplementary text 2 for specific equations). Empirical regressions differed between *Dictyota spp.* and *Lobophora spp.*, and the average conversion was used to calculate the biovolume of macroalgae. Total and exposed biovolumes for all benthic groups were obtained by summing estimates

of volumes on horizontal and vertical surfaces with and without cryptic surfaces, respectively, as described above for 3D surface area.

Biomass of benthic groups

Tissue samples of various sizes (0.7–20 cm³ for erect organisms, 1.7–614 cm² for non-erect organisms, see Online resource 2 for sizes of all individual tissue samples) were collected for all benthic groups (n = 3–8 representative organisms per group) (see Tables S1, S2 for detailed species list and sample sizes) across the surveyed area using different approaches specific to each group (see below). Tissue samples were collected to estimate tissue thickness, ash-free dry weight (AFDW), organic carbon (C_{org}), and organic nitrogen (N_{org}). Samples rich in calcium carbonate (e.g., scleractinian corals, CCA) were collected by chiseling out fragments containing the entire tissue layer (and some underlying calcium carbonate) and subsequently stored in individual 50-mL Falcon tubes. Samples of organisms with embedded skeletal structures (e.g., gorgonians, sponges) were collected by carefully scraping or cutting off a tissue area or volume of known size, using a sharp blade. Sampling of epibionts was avoided and samples were stored in 15-mL falcon tubes. Non-calcifying phototrophs and soft coelobites (e.g., *Didemnum* or hydrozoans) were carefully collected using tweezers and stored in zip lock bags. All samples were photographed *in situ* and transported to the lab for processing within 2 h, where they were photographed again next to a scale. Samples were quickly rinsed in deionized and distilled water (18.2 MΩ-cm type I, Elga Purelab Classic UV) to remove excess salts, and subsequently freeze-dried (Scanvac Coolsafe 55-4, Labogene). Sample DW was determined on a precision scale (± 0.01 mg), after which samples were homogenized (Planetary Ball Mill Pulverisette 5, Laval Lab) for 8 min, at a relative centrifugal force of 22 x *g*, and divided equally into three aliquots. One aliquot was weighed, combusted at 450 °C for 4 h, and weighed again to determine AFDW. The remaining two aliquots were both acidified to remove inorganic C using 4 mol L⁻¹ hydrochloric acid until effervescence ceased (Nieuwenhuize et al. 1994) and analyzed for C_{org} and N_{org} (duplicate measurements) on a carbon, hydrogen, nitrogen, sulphur elemental analyzer (CHNS-EA; Elementar Vario El Cube). H and S contents were not extracted from the output file.

Images of samples were uploaded into ImageJ to estimate surface area and volume using delineation of approximated geometrical shapes (see above). Conversion factors to CT-scanned surface area estimates (Naumann et al. 2009) were applied to samples of corals with grooved or folded surfaces (Online resource 2) to avoid scale differences with the 3D reconstructions used to extrapolate biomass to reef-scale. These corals included *Acropora cervicornis* (factor = 0.95), *Agaricia spp.*, *Mycetophyllia spp.*, and *Pseudodiploria strigosa*. The latter three

species were converted using the ratio determined for the morphologically most similar species *Montipora spp.* (factor = 1.37, Naumann et al. 2009). Smaller irregularities in tissue samples of other non-erect reef organisms did not lead to scale differences with 3D models, except in non-calcifying phototrophs.

To calculate the biomass of non-calcifying phototrophs, we used the same approach as described above for the biovolume of macroalgae, converting 3D surface area to biomass using the empirical regression between canopy height and AFDW for a given area (Figure S5C–F for macroalgae and Figure S6 for turf algae and benthic cyanobacteria). For all erect organisms, whose volumes were measured directly *in situ* (Online resource 7), biomass was estimated by volume-to-biomass conversion factors (Table S1) multiplied by their *in situ*-measured biovolumes. For encrusting sponges, corals, CCA, and other coelobites (e.g., *Didemnum spp.*, hydrozoans), biomass was estimated by surface-to-biomass conversion factors (Table S2) multiplied by their 3D surface area (Online resource 8). The same calculations (see Supplementary text 2) were used to estimate standing stocks of organic carbon (Online resource 9) and nitrogen (Online resource 10), but using weight estimates for C_{org} and N_{org} , respectively (Figures S7, S8), rather than AFDW.

Final abundance metrics (3D surface area, biovolume, biomass) for the seven major benthic groups (gorgonians, scleractinian corals, massive sponges, encrusting sponges, calcifying algae, non-calcifying phototrophs and others) were generated by summing estimates for each benthic group (see Table 1 and Tables S1, S2 for the applied classification) and uncertainties were once again computed analogous to Equation (3). All raw data, equations, and summary statistics are provided in Online resources 1–11.

Statistical analysis

Since relief is commonly used as proxy for structural complexity on reefs, we tested whether relief predicts our measured surface areas (i.e., the summed area of all surfaces present within the reef volume underneath a 1 x 1 m projected reef surface). All data were log transformed prior to analysis to obtain normal distributions (Figure S9). Simple linear regression was used with relief as predictor variable. Dependent variables were either cryptic, exposed, or total surface area per quadrat. Results were then back-transformed for plotting. A roughly uniform spread of residuals verified homoscedasticity of the underlying data.

RESULTS

We characterized the composition of reef communities between 9–14 m water depths along the leeward shore of Curaçao in terms of relative 2D and 3D benthic cover, biovolume, and biomass. We found that surveys taking into account the

three-dimensional nature of coral reefs and reef organisms, and using biomass rather than cover as an abundance metric, greatly altered the relative contribution of dominant benthic groups to overall community composition.

Reef 3D surface areas

The average amount of reef surface area (in $\text{m}^2 \text{m}^{-2}_{\text{planar reef}}$) per site ranged from 5.2 ± 0.4 (mean \pm SE, $n = 16$ quadrats, Jan Thiel) to 7.6 ± 1 ($n = 15$, Jeremi; Figure 1). The island-wide average was $6.0 \pm 0.2 \text{ m}^2 \text{m}^{-2}_{\text{planar reef}}$ ($n = 191$ quadrats in 12 sites). Approximately half of the total reef surface area consisted of cryptic surfaces (island-wide average: $3.3 \pm 0.2 \text{ m}^2 \text{m}^{-2}_{\text{planar reef}}$). The maximum reef surface observed within a quadrat was located at Jeremi and reached $17.4 \text{ m}^2 \text{m}^{-2}_{\text{planar reef}}$, of which 82 % was cryptic surface. Relief as a proxy for reef flatness correlated significantly with total surface area, but explained only 16 % of the variation (Pearson correlation: $R^2 = 0.16$, $n = 191$, $p < 0.001$; Figure S9A,B). This correlation was stronger for cryptic substrates ($R^2 = 0.15$, $n = 191$, $p < 0.001$, Figure 1D) than for exposed substrates ($R^2 = 0.03$, $n = 191$, $p < 0.01$, Figure 1C).

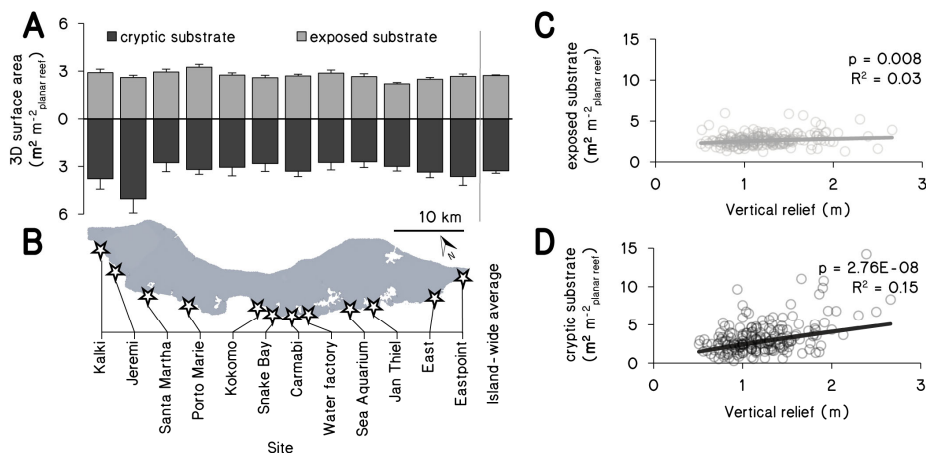


Figure 1. Available 3D-projected surface area in exposed and cryptic habitats along the leeward fringing reefs of Curaçao. Exposed (gray bars, positive y-axis) and cryptic (black bars, negative y-axis) surface areas at 9–14 m depth (A) are shown for 12 sites on Curaçao (B). Bars represent mean values (\pm SE) in $\text{m}^2 \text{m}^{-2}_{\text{planar reef}}$ for each site (based on $n = 16$ quadrats, except Jeremi where $n = 15$), and all sites combined ($n = 191$). Also shown are correlations between exposed (C) or cryptic (D) substrate (y-axis) and vertical relief (i.e., distance between highest and lowest point in contact with seawater, x-axis) for all quadrats ($n = 191$).

Reef benthic community composition

The estimated contributions of different benthic groups to the total reef benthos greatly depended on the abundance metric used (2D/3D cover, biovolume, or biomass) (Figure 2, Table 1).

2D projected cover

According to a traditional assessment, using the percent relative cover estimated by 2D projection of exposed reef surfaces, the most abundant benthic groups were non-calcifying phototrophs (52 ± 2 %) and scleractinian corals (32 ± 2 %) (Figure 2A; Figure 3A,B; Table 1). Lowest cover was found for encrusting sponges (0.07 ± 0.03 %; Figure 3F) and massive sponges (1.5 ± 0.3 %; Figure 3E). Note that this traditional 2D relative cover approach does not include benthic communities in cryptic reef habitats and only assesses the exposed reef surfaces visible from photographs taken above the reef (Figure 2A).

3D total cover

When considering the relative contribution to 3D (exposed and cryptic) reef surface areas, non-calcifying phototrophs were still the largest benthic group (25 ± 5 % of total 3D surface area) and dominated the exposed reef surface together with scleractinian corals (11 ± 2 %) (Figure 2B, Figure 3A,B, Table 1). The second and third largest benthic groups were encrusting sponges (20 ± 8 %) and calcifying algae (19 ± 3 %) that dominated the reef's cryptic surface areas (Figure 2B, Figure 3D,F, Table 1). The contribution of organisms with soft, erect morphologies (i.e., massive sponges and gorgonians) to 3D surface area was minor in all reef habitats across the island (Figure 2B, Figure 3C,E).

Biovolume

When community abundances are expressed as biovolumes, massive sponges (22 ± 8 % of total biovolume) and gorgonians (6 ± 1 %) became profoundly more dominant on the exposed reef surface (Figure 2C, Table 1). The contributions of non-calcifying phototrophs (20 ± 2 %) and scleractinian corals (8 ± 2 %) decreased in comparison to 2D cover and 3D surface area measurements (Figure 2A–C, Figure 3A,B, Table 1). The biovolume of massive sponges displayed considerable variation among sites, with highest biovolume at Carmabi in the center of the island and lowest biovolume on the Eastern side. The biovolume of the cryptic community was dominated almost exclusively by encrusting sponges (33 ± 15 %), which showed a more consistent abundance across the island (Figure 2C).

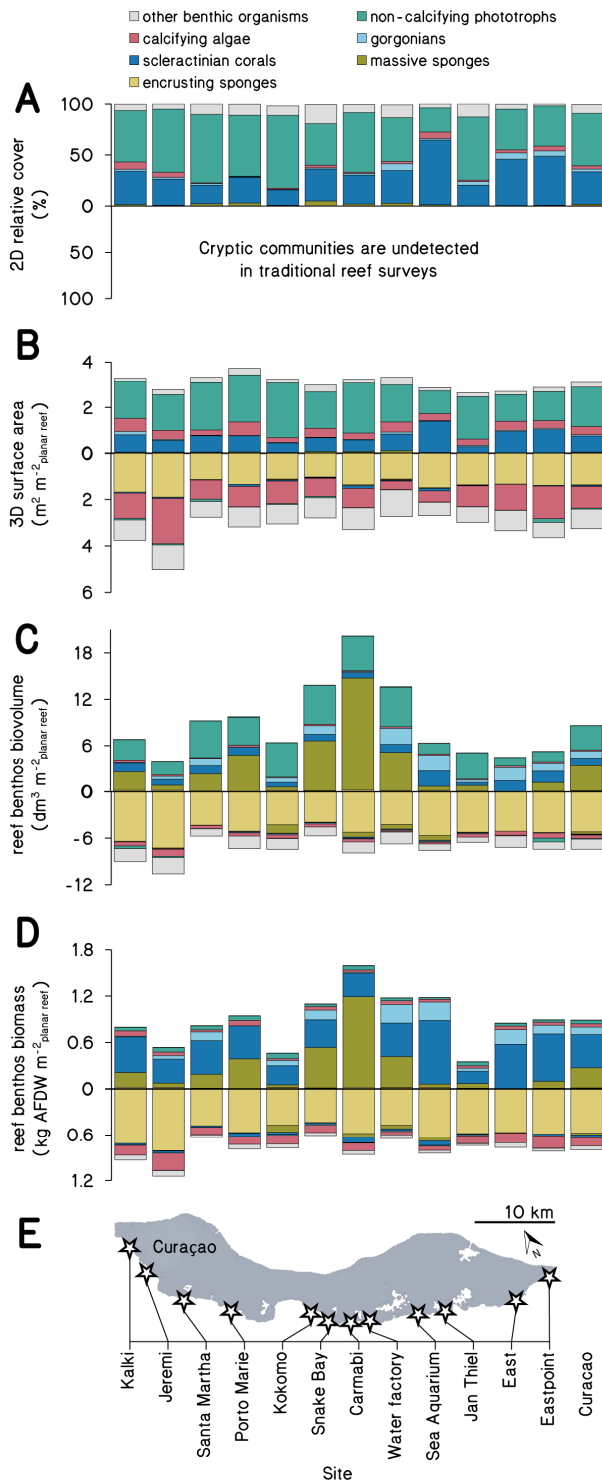


Figure 2. Size and composition of the reef benthos using different 2D and 3D abundance metrics. Mean community sizes (\pm SE) in exposed (positive y-axes) and cryptic (negative y-axes) reef habitats at 9–14 m depth at 12 sites are shown as 2D relative cover in % of total benthos (A), 3D covered surface area in $\text{m}^2 \text{m}^{-2} \text{planar reef}$ (B), reef benthos biovolume in $\text{dm}^3 \text{m}^{-2} \text{planar reef}$ (C), and reef benthos biomass in $\text{kg ash-free dry weight (AFDW) m}^{-2} \text{planar reef}$ (D) along the leeward shore of Curaçao (E). $n = 16$ quadrats per site, except Jeremi where $n = 15$. SE's are provided in Table 1. In panel (A), the category “other benthic organisms” also includes exposed sediment and rubble.

2

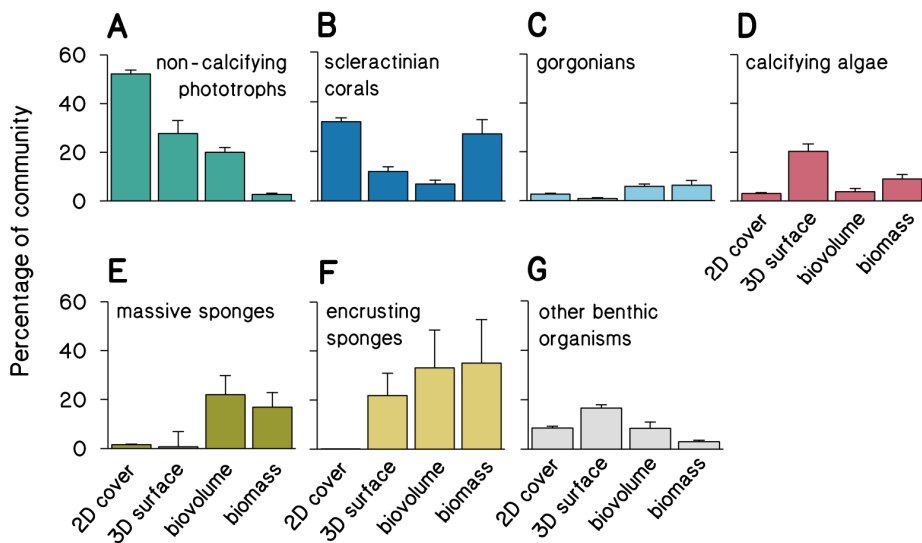


Figure 3. Relative contributions of benthic groups using different 2D and 3D abundance metrics. Shown are relative proportions (mean \pm SE) of each benthic group to the total benthic reef community size in terms of 2D relative cover, 3D surface area, biovolume, and biomass ($n = 191$ quadrats, see Tables S1 and S2 for sample sizes of metric conversions).

Biomass

When expressed as biomass, the reef community composition was generally similar to the reef's community composition expressed as biovolume (compare Figure 2C and 2D). The clearest difference between biomass and biovolume estimations is the increase in contribution of scleractinian corals ($27 \pm 6\%$ of total biomass) and the diminished contribution of non-calcifying phototrophs ($< 5\%$) to total benthic reef biomass (Figure 2C,D, Figure 3A,B, Table 1). Notably, more than half of the reef biomass was comprised of encrusting ($35 \pm 18\%$) and massive ($17 \pm 6\%$) sponges (Figure 3E,F).

The composition of reef communities in terms of organic carbon closely resembled our findings for biomass (Table 1), and is therefore not explicitly plotted or discussed. Volume-to-biomass and surface-to-biomass conversions are provided in Figure S7, Table S1 and Figure S8, Table S2, respectively. Additional data underlying our results (e.g., site coordinates, canopy heights of non-calcifying phototrophs, relative cover on different surface types, species-specific biomass conversions, standing stocks and tissue contents of organic nitrogen) are provided in Online resources 2–11.

Table 2. Total benthic community size in terms of 3D surface area, biovolume, biomass (ash-free dry weight), and organic carbon. Values are mean \pm SE. Shown are absolute values (abs) and relative proportions (rel) of exposed (i.e., exposed to sunlight) and cryptic reef communities. See Tables S1, S2 and *Methods* for sample sizes of underlying measurements.

habitat		3D	tissue	ash-free	organic
		surface area	volume	dry weight	carbon
		[m ² m ⁻² planar reef]	[dm ³ m ⁻² planar reef]	[kg m ⁻² planar reef]	[kg m ⁻² planar reef]
total reef		6.36 \pm 0.81	16.01 \pm 2.83	1.68 \pm 0.33	0.67 \pm 0.15
exposed reef	abs	3.10 \pm 0.19	8.60 \pm 1.28	0.89 \pm 0.12	0.33 \pm 0.05
	rel	0.49 \pm 0.03	0.54 \pm 0.08	0.53 \pm 0.07	0.49 \pm 0.08
cryptic reef	abs	3.26 \pm 0.13	7.42 \pm 1.24	0.79 \pm 0.17	0.34 \pm 0.08
	rel	0.51 \pm 0.02	0.46 \pm 0.08	0.47 \pm 0.10	0.51 \pm 0.12

DISCUSSION

The divided community structure of coral reef frameworks

Coral reefs form some of the most diverse ecosystems of our planet, and their biodiversity and ecosystem functioning is severely threatened by coastal eutrophication and climate change (Hughes et al. 2003; Hoegh-Guldberg et al. 2007; Carpenter et al. 2008). Yet, progress in understanding their ecosystem functioning has been strongly limited by a lack of quantitative data on the relative abundances of the different functional groups in these complex ecosystems. This study represents a comprehensive assessment of the community composition and size of both the exposed and cryptic surfaces in a coral reef ecosystem. Our results show that approximately half of the total reef surface area, biovolume, and biomass of the fringing reefs of Curaçao resides in “hidden” cryptic spaces (Figures 1, 2). Important to note is that the composition of the benthic groups in this cryptic habitat is markedly different from the exposed part of the ecosystem. Although very few studies have been conducted on cryptic reef communities, Caribbean (Jackson and Winston 1982; Scheffers 2005; van Duyl et al. 2006), Red Sea (Wunsch 1999; Richter et al. 2001) and Indonesian reefs (de Goeij and van Duyl 2007) show a consistent dominance of encrusting sponges, calcifying algae, and other suspension feeders (e.g., bivalves, hydrozoans, polychaetes, tunicates). These cryptic communities act as major regenerators of organic (Richter et al. 2001; de Goeij and van Duyl 2007; de Goeij et al. 2013) and inorganic nutrients (Tribble et al. 1990; Gast et al. 1998; Rasheed et al. 2002) within the oligotrophic reef ecosystem. Consequently, the lack of integration of the cryptic habitat in reef-scale assessments seriously hampers our understanding of coral community composition, species interactions, biogeochemical cycling, and thus our understanding of overall coral reef ecosystem functioning in changing oceans. Proper baselines for cryptic reef communities are also needed because coral reefs

worldwide are reportedly flattening (Alvarez-Filip et al. 2009; Newman et al. 2015; Bellwood et al. 2018; Magel et al. 2019; Tebbett et al. 2019). Given that a reduction in reef relief is associated with a decrease of cryptic reef surfaces (Figure 1D), our findings suggest that ongoing flattening of reefs could primarily diminish the largely undescribed cryptic habitats. Further, the lack of correlation between relief and exposed surface area (Figure 1C) implies that traditional monitoring of reef rugosity could fail to detect this decrease in structural complexity.

Key insights and implications

Including the cryptic habitat in reef assessments indicates that most reef biomass in our study area is represented by sponges, with other major contributions to community biomass by scleractinian corals, gorgonians, and calcifying algae (Figure 3, Figure 4B; Table 1). Sponges, however, cover only 2 % of all exposed substrates along the reef slopes of Curaçao at the surveyed depths (Online resource 6) and are therefore largely overlooked in traditional 2D reef surveys (Figure 2A, Figure 4). Community biomass on the exposed part of the reef is mainly dominated by massive sponges (Figure 2D, positive y-axis), whereas encrusting sponges dominate the cryptic habitat (Figure 2D, negative y-axis) and can represent a staggering 35 % of the total biomass in benthic reef communities (Figure 3F). This number coheres with recent studies describing how encrusting sponges drive large and important nutrient fluxes between cryptic and exposed reef habitats (de Goeij et al. 2013; Rix et al. 2016; Lesser and Slattery 2020). Specifically, they turn dissolved organic carbon, the largest source of organic matter, into consumable detritus entering the food web, a pathway called the sponge loop (de Goeij et al. 2013). Cycling rates through this sponge loop were estimated to be comparable to overall coral reef primary production. These fluxes were based solely on carbon cycling through cryptic, encrusting sponges under the assumption that 1 m² of reef concealed 2.8 m² of cryptic surface (de Goeij and van Duyl 2007), which is very close to the island-wide 3.3 m² per quadrat determined in this study. The extent of dissolved organic carbon cycling through massive (i.e., non-encrusting) sponges and the overall ecological role of sponges under changing ocean conditions are still under debate (e.g., de Goeij et al. 2017; McMurray et al. 2018; Pawlik and McMurray 2020), which illustrates the current lack of knowledge on these hitherto largely neglected key ecosystem drivers.

The biomass of non-calcifying phototrophs was an order of magnitude lower than scleractinian corals despite dominant macroalgal (2D) surface cover (Figure 4). This was caused foremost by low tissue weights of macroalgae, turf algae, and benthic cyanobacterial mats compared to other benthic taxa (Odum and Odum 1955; Hatcher 1988; Miller et al. 2003). For instance, the AFDW of the heaviest alga *Lobophora spp.* covering one square meter of reef substrate was only 70 g m⁻²

and contained 30 g m⁻² of organic carbon, which is an order of magnitude lower than most other benthic organisms (Table S2). Miller et al. (2003) compared relative cover and biomass of macroalgae in the Florida Keys in 1998 and 1999, reporting 20 and 65 % cover, and biomasses of 16 and 60 g m⁻²_{planar reef}, respectively. Our estimates for macroalgae (29 % cover; 45 g m⁻²_{planar reef}), turf algae (19 % cover; 10 g m⁻²_{planar reef}), and all non-calcifying phototrophs (52 % cover; 56 g m⁻²_{planar reef}) fall closely within these ranges (Table 1). Importantly, the canopy height of these phototrophs can vary dramatically depending on nutrient loads and grazing pressures (Lapointe et al. 1997; Littler et al. 2006), which affects their biomass but not surface cover. Although we incorporated variation in canopy height in our analysis, it had limited influence on the low contribution of non-calcifying phototrophs to overall reef community biomass, particularly for *Lobophora* spp. (Figure S5D,F, but see Steneck and Dethier 1994). The relatively low biomass but high cover of non-calcifying phototrophs is accompanied by major contributions of macroalgae to reef-wide primary production (Wanders 1976; Hatcher 1988) and nutrient cycling (Haas et al. 2010; Mueller et al. 2014b). The co-occurrence of a high productivity but low biomass is likely due to the high turnover rates of macroalgae, turf algae and cyanobacterial mats, as they are often heavily grazed (Ferrari et al. 2012) and can release substantial amounts of dissolved organic matter (Mueller et al. 2014b). Hence, although their turnover rates cannot be estimated from snapshots of community composition, the low biomass contributions of non-calcifying phototrophs do not imply that they play only a minor role in ecosystem productivity.

2

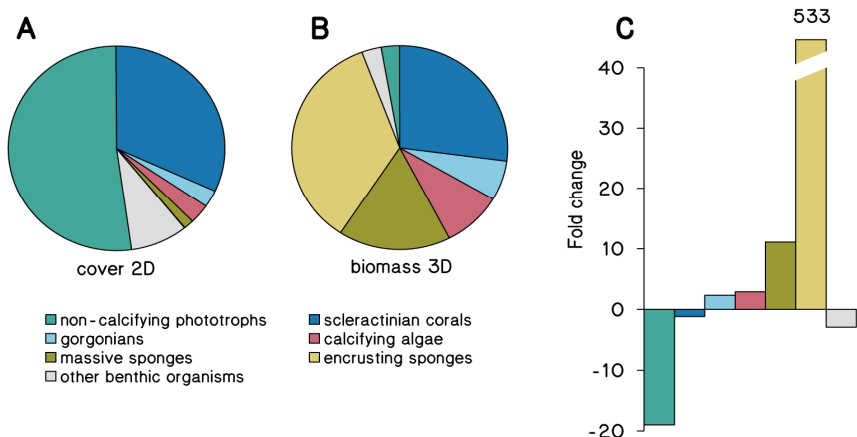


Figure 4. Relative composition of the benthic reef community in terms of cover and biomass. Shown are relative proportions of the different benthic groups to benthic reef community cover in 2D (A), and whole reef community biomass in 3D (B), as well as the fold change from cover to biomass (C) (n = 191 quadrats).

Surveying reefs in 3D

The abundance metrics portrayed here have different strengths and weaknesses. Organic biomass and element analysis (e.g., C, N, P) estimates—though limited in scaling opportunity—provide the most comprehensive insights into the standing stocks and biogeochemical cycling of energy and (in)organic nutrients at aquatic and terrestrial ecosystem scale (Diaz and Rützler 2001; Dubinsky and Stambler 2010; Atkinson 2011; Le Toan et al. 2011). The assessment of community biovolume requires less effort, but introduces additional challenges, such as measuring the average protrusion of coral tissue into the underlying skeleton, empty spaces in tissues of massive sponges, or the free space between filaments of turf algae and benthic cyanobacteria. All are subject to assumptions in this study and would need improved measures to gain accuracy and confidence. At the other end of the spectrum, traditional 2D surveys are fast, cost-effective, and scalable (Gardner et al. 2003; De'ath et al. 2012) but incomplete to varying degrees depending on the reef's structural complexity. While we acknowledge that many reef assessments span much larger survey areas compared to this study, we support previous recommendations to assess reefs in 3D (González-Rivero et al. 2014; Burns et al. 2015; Ferrari et al. 2016). This step is substantially facilitated by the recent surge in studies validating structure-from-motion photogrammetry as an appropriate tool to generate digital twins of reefs (Figueira et al. 2015; Leon et al. 2015; Guo et al. 2016; Burns and Delparte 2017). We show that 3D surface areas can be estimated from these models, automatically assigned into exposed (i.e., visible) and cryptic (i.e., inverted or shaded) reef surfaces, and combined with traditional coral point counts on these surfaces to estimate 3D surface cover. However, for trophic modeling, 3D surface cover alone is still not sufficiently representative for the contribution of individual taxa to reef communities (Figure 2B,D). Community data can be converted to biochemical proportions using conversion factors from the extending literature from several worldwide coral reef locations (Brey et al. 2010; Stratmann et al. 2020). Adopting such a strategy would require relatively little additional effort, while dramatically increasing the ecological resolution of ongoing accounts of coral reef communities.

Limitations & conclusion

There are some important limitations regarding our biomass estimates. First, they must be considered conservative estimations, since despite our best efforts to quantify all existing benthic organisms, some biota residing within inaccessible cavities and endolithic taxa, such as bioeroding sponges or other burrowing organisms, were not included due to logistical constraints and to avoid destructive practices associated with such measurements (Fang et al. 2013). Complementary approaches, such as the use of artificial substrates (Leray and Knowlton 2015;

Vicente et al. 2021), could greatly improve the identification and quantification of these cryptic communities. Second, cryptic sediments were not quantified in this study. Although exposed sediment cover was low (5.7 %) in our survey areas (Online resource 6), cryptic sediments can account for up to 40 % of the substrate in coral reef cavities (de Goeij and van Duyl 2007), while data on the standing stocks of local sediment micro- and macrofaunal communities are lacking. Third, we acknowledge that our sampling approach (e.g., the selection of surfaces for vertical and cryptic reef assessments) may have caused biases in our community estimations and further improvements in randomization of the spatial sampling methods are needed to monitor changes in 3D reef communities over time (e.g., Smith et al. 2017). Our data therefore serve as a first example of biomass distributions in Caribbean reefs or even tropical coral reefs in general. Here described patterns of sponge-dominance are in line with previous reports from both exposed (Pawlik 2011; Bell et al. 2013) and cryptic reef habitats (Meesters et al. 1991; Scheffers et al. 2010), including Red Sea reefs (Richter and Wunsch 1999). Yet, a variety of geographical areas need to be surveyed using similar approaches to validate our finding that sponges dominate standing stocks of benthic biomass on Caribbean coral reefs (Rützler 1978). Lastly, motile fauna and pelagic biota represent important components of coral reefs that were not assessed in this study. While community data on motile invertebrate abundance does not exist for the studied area, local fish biomass has been estimated to account for $0.130 \pm 0.012 \text{ kg m}^{-2}_{\text{planar reef}}$ (Sandin et al. 2008b). Bacterio- and phytoplankton standing stocks on local reefs amount to $< 0.001 \text{ kg m}^{-2}_{\text{planar reef}}$ (Lesser et al. 2020), assuming an average water depth of 10 m. While these pelagic communities are one to four orders of magnitude smaller than the benthic communities determined in this study ($1.7 \pm 0.3 \text{ kg per quadrat}$), they should also be incorporated into standing stock assessments, along with motile invertebrates, to improve our understanding of how benthic-pelagic interactions shape marine ecosystems and their response to environmental change.

We show that different abundance metrics (2D cover, 3D surface area, biovolume, biomass) lead to markedly different perspectives on benthic reef community composition. These different abundance metrics serve different ecological questions. For example, conventional 2D approaches may provide the best balance between accuracy, scale, and required resources if the goal is to indicate general reef health based on the relative proportions of, for example, scleractinian corals and macroalgae. But the same conventional approach structurally overestimates the biomass contribution of conspicuous primary producers (i.e., macroalgae, turf algae), while underestimating the contributions of reef taxa with erect morphologies (i.e., gorgonians, massive sponges) that have important functions in nutrient cycling, biodiversity, and reef productivity (Ferrier-

Pagès and Gattuso 1998; Maldonado et al. 2012; de Goeij et al. 2017). To move beyond limited descriptions of the current state of reefs, and incorporate (biogeochemical) processes driving reef states, newly emerging 3D approaches using photogrammetry (González-Rivero et al. 2014; Burns et al. 2015; Ferrari et al. 2016) mostly overcome this limitation, albeit they do not capture the cryptic habitat specifically, potentially rendering large parts of the reef system undetected, such as crevices and holes not obvious to an observer swimming over a reef. Biomass and organic carbon stocks determined in this study will strengthen estimates of ecosystem productivity and biogeochemical cycling in coral reefs, and our metric conversions can be used to augment reef surveys at other Caribbean locations, to ultimately improve predictions of how complex benthic ecosystems develop in the Anthropocene.

Acknowledgements

We thank Eva de Rijke, Fabien Pocino, Gloria Mariño, Jorien Schoorl, Kelly Latijnhouwers, Kristen Marhaver, Martijn Bart, Meggie Hudspith, Mischa Streekstra, Nina Leestemaker, Rutger van Haal, Sara Campana, Titus Rombouts, Valerie Chamberland, as well as the Carmabi Research Foundation for their support with laboratory, fieldwork, or model processing activities. We also thank the Sea Aquarium on Curaçao for access to their dive sites, the Blue Bay Diving Center for discounted dive tanks, and NVIDIA Corporation for donating the Titan Xp GPU used for this research. This work was funded by the European Research Council under the European Union's Horizon 2020 research and innovation programme (Starting Grant agreement # 715513 to JMdG).

SUPPLEMENTARY INFORMATION

Supplementary texts

Text 1: Simulating direct light to discern exposed and cryptic reef surfaces

Cryptic habitats are broadly defined in the literature, ranging from large caves, to crevices and holes, to the spaces between sand grains (Choi and Ginsburg 1983; Ginsburg 1983). We defined exposed and cryptic surfaces solely based on their orientation, whereby exposed surfaces are directly visible for a human observer swimming over the reef whereas cryptic surfaces are out of direct view because they are hidden behind exposed surfaces. We aimed at automating the classification of the 3D reconstructed surfaces into either *exposed* or *cryptic* according to the above criteria. For this purpose, we employed the Ambient Occlusion (Landis 2002) algorithm which is a 3D object shading and rendering technique in computer graphics. It estimates the percentage of occlusion of direct light by nearby objects according to:

$$(1) \quad AO(x, \vec{n}) = \frac{1}{\pi} \cdot \int_{\vec{\omega} \in \Omega} V(x, \vec{\omega}) (\vec{n} \cdot \vec{\omega}) d\vec{\omega}$$

where \vec{n} is the normal vector of the surface tangent and V is the visibility function along the direction of $\vec{\omega}$. The function returns the value 0 if the surface is fully occluded, and 1 if the surface is fully exposed. We used the Meshlab implementation of the AO algorithm (Sabbadin et al. 2016) with 128 simulated 60-degree conical sources and a directional bias of 0.5. To calibrate the annotation into exposed and cryptic surfaces, we first applied the AO algorithm on selected 3D reconstructions of exposed reef tops and cryptic overhangs, which yielded the brighter and darker populations of exposure indices, respectively, in Figure S3. The exposure threshold for automatic annotations was selected where the two frequency histograms meet. This threshold provides the maximum likelihood to correctly annotate surface elements of unknown type for an expected bimodal distribution. While this approach can correctly annotate digital surfaces based on their orientation and the presence of surfaces in their surroundings, our definition of cryptic habitats is limited and would benefit from ecological assessments of how light mediates the spatial extent of exposed and cryptic reef communities.

Text 2. Equations used to calculate 3D surface area, biovolume, and biomass of benthic coral reef organisms.

3D surface area (SA) of benthic group i on horizontal (ho), vertical (ve), and cryptic (cr) substrates, with A as substrate surface area determined by 3D reconstructions (see Methods) and C as relative cover, was calculated by:

$$(2) \quad SA_{ho,i} = A_{ho,i} \cdot C_{ho,i}$$

$$(3) \quad SA_{ve,i} = A_{ve,i} \cdot C_{ve,i}$$

$$(4) \quad SA_{cr,i} = A_{cr,i} \cdot C_{cr,i}$$

Uncertainty (δ) for 3D surface area on individual substrates (shown here for cryptic substrates) was propagated according to:

$$(5) \quad \delta SA_{cr,i} = SA_{cr,i} \cdot \sqrt{\left(\frac{\delta A_{cr,i}}{A_{cr,i}}\right)^2 + \left(\frac{\delta C_{cr,i}}{C_{cr,i}}\right)^2}.$$

Total 3D surface area (TSA) of benthic group i and its uncertainty were calculated by:

$$(6) \quad TSA_i = SA_{ho,i} + SA_{ve,i} + SA_{cr,i}$$

$$(7) \quad \delta TSA_i = \sqrt{(\delta SA_{ho,i})^2 + (\delta SA_{ve,i})^2 + (\delta SA_{cr,i})^2}.$$

Exposed 3D surface area (TSA_E) of benthic group i and its uncertainty were calculated by:

$$(8) \quad TSA_{E,i} = SA_{ho,i} + SA_{ve,i}$$

$$(9) \quad \delta TSA_{E,i} = \sqrt{(\delta SA_{ho,i})^2 + (\delta SA_{ve,i})^2}.$$

Volume of organic tissue (V) for non-erect, roughly isometric organisms (including scleractinian corals) on individual substrates (shown here for horizontal surfaces) and its uncertainty, where d is the tissue thickness, were calculated by:

$$(10) \quad V_{ho,i} = TSA_{ho,i} \cdot d_{ho,i}$$

$$(11) \quad \delta V_{ho,i} = V_{ho,i} \cdot \sqrt{\left(\frac{\delta TSA_{ho,i}}{TSA_{ho,i}}\right)^2 + \left(\frac{\delta d_{ho,i}}{d_{ho,i}}\right)^2}.$$

Volume for macroalgae (denoted by M) on individual substrates (shown here for horizontal surfaces) and its uncertainty, with D denoting *Dictyota spp.* and L denoting *Lobophora spp.*, while vCH_D and vCH_L represent the functions of area-normalized tissue volume by canopy height (CH) for *Dictyota* (Figure S5A) and *Lobophora* (Figure S5B), respectively, were calculated by:

$$(12) \quad V_{ho,M} = TSA_{ho,M} \cdot \frac{vCH_D(CH_{ho,D}) + vCH_L(CH_{ho,L})}{2}$$

$$(13) \quad \delta V_{ho,M} = V_{ho,M} \cdot \sqrt{\left(\frac{\delta TSA_{ho,M}}{TSA_{ho,M}}\right)^2 + (\delta vCH_{ho,M})^2},$$

where $\delta vCH_{ho,m}$ is obtained according to:

$$(14) \quad \delta vCH_{ho,M} = \frac{(vCH_D(CH_{ho,M} + \delta CH_{ho,M}) - vCH_D(CH_{ho,M})) + (vCH_L(CH_{ho,M} + \delta CH_{ho,M}) - vCH_L(CH_{ho,M}))}{vCH_D(CH_{ho,M}) + vCH_L(CH_{ho,M})}.$$

Total volume of benthic group i and its uncertainty were calculated by:

$$(15) \quad V_i = V_{ho,i} + V_{ve,i} + V_{cr,i}$$

$$(16) \quad \delta V_i = \sqrt{(\delta V_{ho,i})^2 + (\delta V_{ve,i})^2 + (\delta V_{cr,i})^2}.$$

Exposed volume (V_E) of benthic group i and its uncertainty were calculated by:

$$(17) \quad V_{E,i} = V_{ho,i} + V_{ve,i}$$

$$(18) \quad \delta V_{E,i} = \sqrt{(\delta V_{ho,i})^2 + (\delta V_{ve,i})^2}$$

Biomass of organic tissue (B) for erect organisms (gorgonians and massive sponges) on individual substrates (shown here for vertical surfaces) and its uncertainty, where mv is the biomass normalized to tissue volume, were calculated by:

$$(19) \quad B_{ve,i} = V_{ve,i} \cdot mv_{ve,i}$$

$$(20) \quad \delta B_{ve,i} = V_{ve,i} \cdot \sqrt{\left(\frac{\delta V_{ve,i}}{V_{ve,i}}\right)^2 + \left(\frac{\delta mv_{ve,i}}{mv_{ve,i}}\right)^2}$$

Biomass of organic tissue (B) for non-erect, roughly isometric organisms (including scleractinian corals) on individual substrates (shown here for horizontal surfaces) and its uncertainty, where ms is the biomass normalized to surface area, were calculated by:

$$(21) \quad B_{ho,i} = TSA_{ho,i} \cdot ms_{ho,i}$$

$$(22) \quad \delta B_{ho,i} = B_{ho,i} \cdot \sqrt{\left(\frac{\delta TSA_{ho,i}}{TSA_{ho,i}}\right)^2 + \left(\frac{\delta ms_{ho,i}}{ms_{ho,i}}\right)^2}$$

Organic biomass for turf algae or benthic cyanobacteria on individual substrates (shown here for horizontal surfaces) and its uncertainty, with mCH_i representing the area-normalized biomass (Figure S6A,B), were calculated by:

$$(23) \quad B_{ho,i} = TSA_{ho,i} \cdot mCH_i(CH_{ho,i})$$

$$(24) \quad \delta B_{ho,i} = B_{ho,i} \cdot \sqrt{\left(\frac{\delta TSA_{ho,i}}{TSA_{ho,i}}\right)^2 + (\delta mCH_{ho,i})^2}$$

where $\delta mCH_{ho,i}$ is obtained according to:

$$(25) \quad \delta mCH_{ho,i} = \frac{(mCH_i(CH_{ho,i} + \delta CH_{ho,i}) - mCH_i(CH_{ho,i}))}{mCH_i(CH_{ho,i})}$$

Organic biomass for macroalgae on individual substrates (shown here for horizontal surfaces) and its uncertainty, with mCH_D and mCH_L representing the functions of area-normalized biomass by canopy height for *Dictyota* (Figure S5C) and *Lobophora* (Figure S5D), respectively, were calculated by:

$$(26) \quad B_{ho,M} = TSA_{ho,M} \cdot \frac{mCH_D(CH_{ho,M}) + mCH_L(CH_{ho,M})}{2}$$

$$(27) \quad \delta B_{ho,M} = B_{ho,M} \cdot \sqrt{\left(\frac{\delta TSA_{ho,M}}{TSA_{ho,M}}\right)^2 + (\delta mCH_{ho,M})^2}$$

where $\delta mCH_{ho,M}$ is obtained according to:

$$(28) \quad \delta mCH_{ho,M} = \frac{(mCH_D(CH_{ho,M} + \delta CH_{ho,M}) - mCH_D(CH_{ho,M})) + (mCH_L(CH_{ho,M} + \delta CH_{ho,M}) - mCH_L(CH_{ho,M}))}{mCH_D(CH_{ho,M}) + mCH_L(CH_{ho,M})}$$

Total organic biomass of benthic group i and its uncertainty were calculated by:

$$(29) \quad B_i = B_{ho,i} + B_{ve,i} + B_{cr,i}$$

$$(30) \quad \delta B_i = \sqrt{(\delta B_{ho,i})^2 + (\delta B_{ve,i})^2 + (\delta B_{cr,i})^2}.$$

Exposed organic biomass (B_E) of benthic group i and its uncertainty were calculated by:

$$(31) \quad B_{E,i} = B_{ho,i} + B_{ve,i}$$

$$(32) \quad \delta B_{E,i} = \sqrt{(\delta B_{ho,i})^2 + (\delta B_{ve,i})^2}.$$

Organic carbon stocks and associated uncertainties were calculated using equations 19 – 32, while replacing area- and volume-normalized organic biomass with area- and volume-normalized organic carbon mass (Tables S1, S2). For non-calcifying phototrophs, the relationships mCH_i were also replaced with the functions describing area-normalized organic carbon mass by canopy height (Figure S5E,F for *Dictyota spp.* and *Lobophora spp.*, Figure S6C,D for turf algae and benthic cyanobacteria).

Supplementary figures



Figure S1. Locations of the 12 surveyed coral reef stations on Curaçao in the Southern Caribbean. Coordinates are provided in Online resource 11.

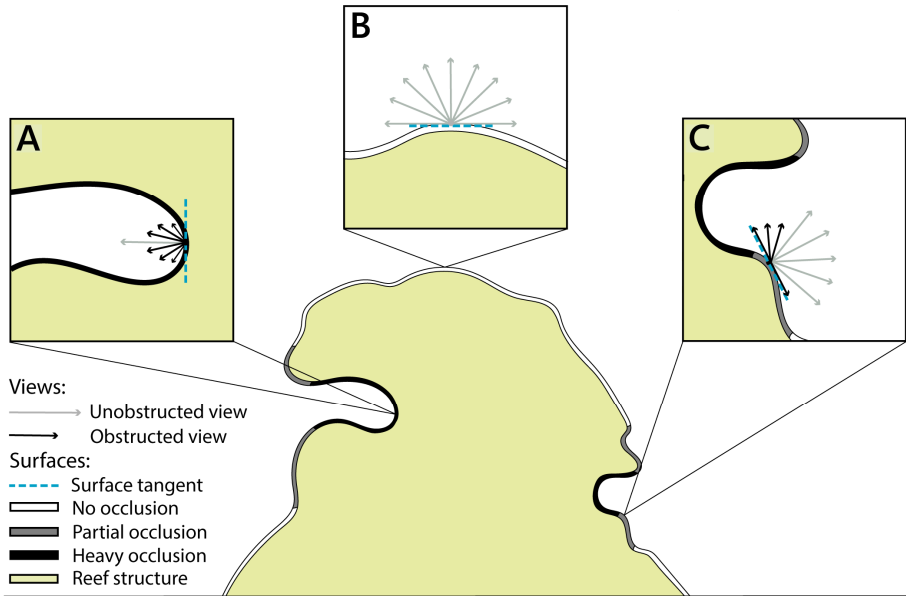


Figure S2. Illustration of reef structure surface classification using an Ambient Occlusion algorithm. For each element of the modeled surface, the exposure index is computed as the normalized sum of the unobstructed views, divided by the total number of views ($n = 256$ views per surface element). As a result, cryptic surfaces (as in surface **A**) will exhibit a lower exposure index than those surfaces completely exposed or with low occlusion (e.g., surfaces **B** & **C**).

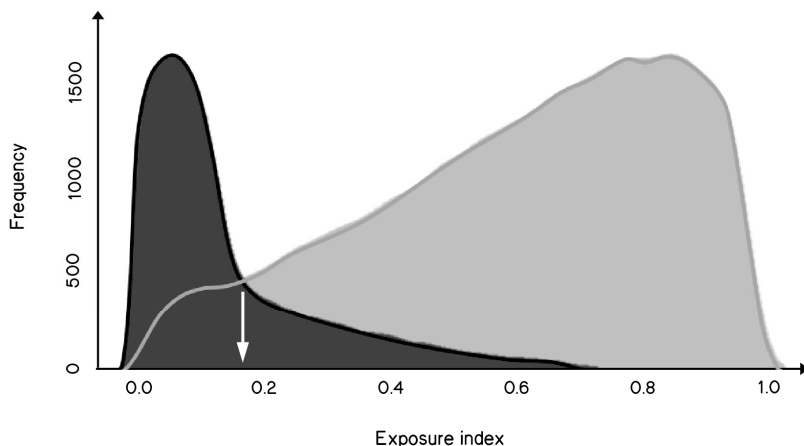


Figure S3. Frequency distributions of exposure indices for the calibration of cryptic and exposed surface annotation. Typical exposure indices of cryptic surfaces (dark gray) were obtained by applying the Ambient Occlusion algorithm to 3D models of cavity surfaces ($n = 3$). Indices of exposed reef surfaces (light gray) were obtained from 3D models of flat reef tops ($n = 3$). Each model consists of tens of thousands of individual surface elements that each return an exposure index. Values towards 0 mean that the modeled surface is predominantly shaded by other reef surfaces (see Figure S2A), while values towards 1 mean that the surface element is largely exposed, that is, in direct line of site to an external observer above or next to the reef (see Figure S2B,C). The intersection point between the two distributions (17.5 %, white arrow) was used as a threshold to automatically annotate all surface elements in our 191 reef reconstructions to either cryptic or exposed substrate.

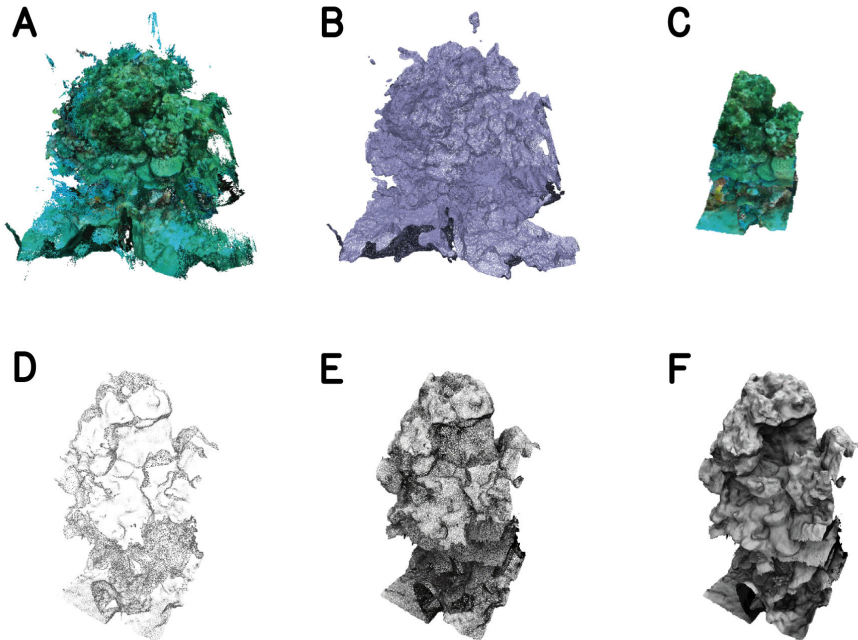


Figure S4. Processing steps of structure-from-motion based 3D reconstructions: (A) high density 3D point cloud, (B) untextured surface mesh obtained from the point cloud and (C) fully textured 3D model of the sample quadrat cropped to 1m x 1m. Light exposure was estimated by (D) resampling the high-density point cloud to 5 mm, (E) smoothing the untextured surface with a two-step Gaussian filter and (F) applying the ambient occlusion algorithm. Note that cryptic surfaces appear darker than exposed surfaces.

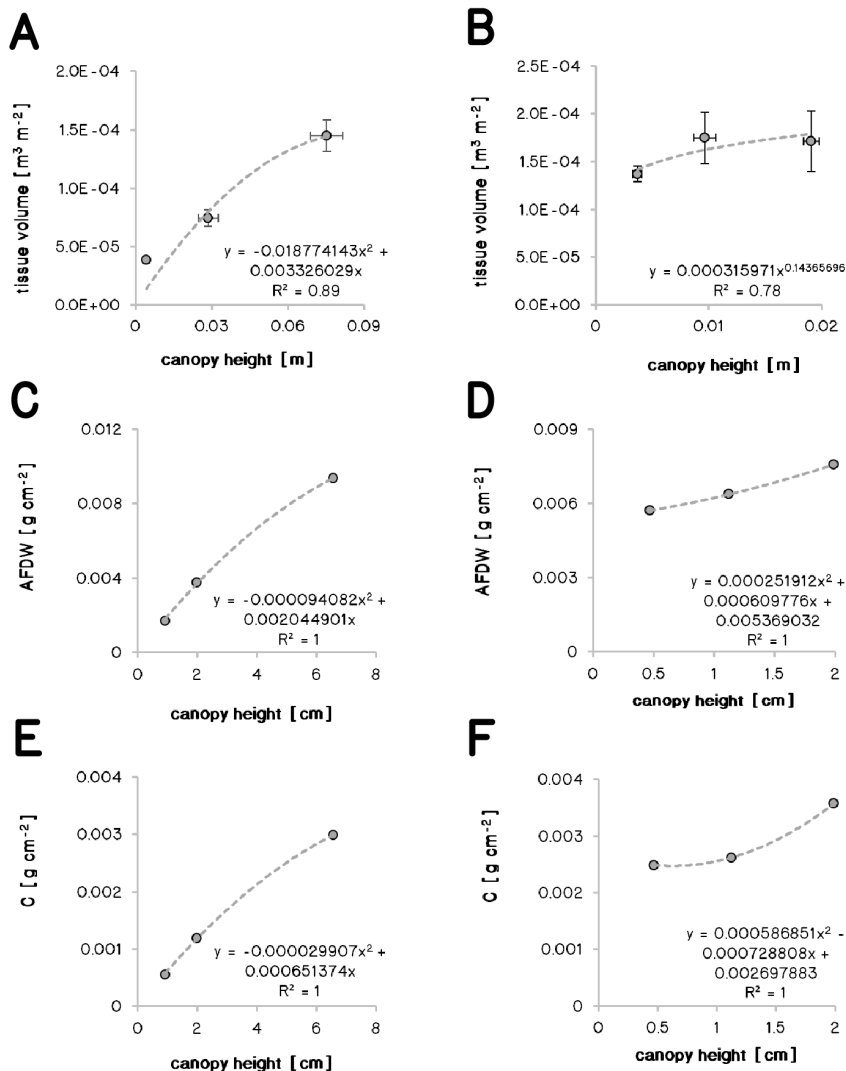
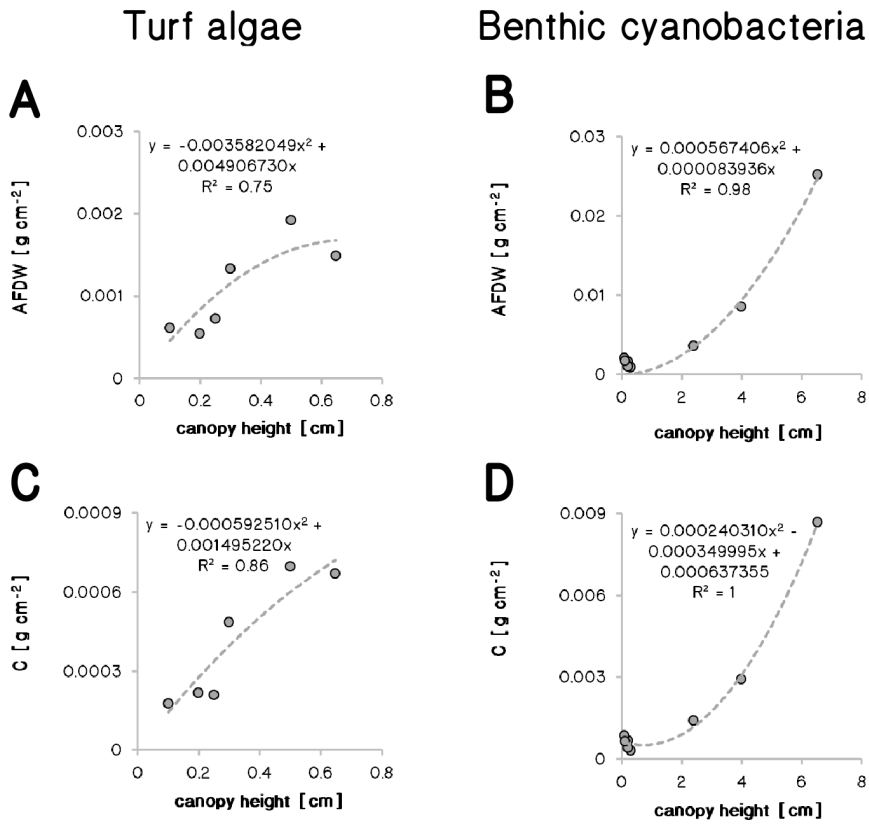
*Dictyota spp.**Lobophora spp.*

Figure S5. Relationships of algal canopy height and area-normalized tissue volume (A, B, $n = 9$, error bars are SE), area-normalized ash-free dry weight (AFDW, C, D, $n = 3$), and area-normalized organic carbon weight (E, F, $n = 3$) for *Dictyota spp.* (A, C, E) and *Lobophora spp.* (B, D, F, see Tables S2 and S4 for underlying data).



2

Figure S6. Relationship of algal canopy height with area-normalized ash-free dry weight (AFDW, **A**, **B**), and organic carbon weight (**C**, **D**) for turf algae (**A**, **C**, n = 6) and benthic cyanobacterial mats (**B**, **D**, n = 8).

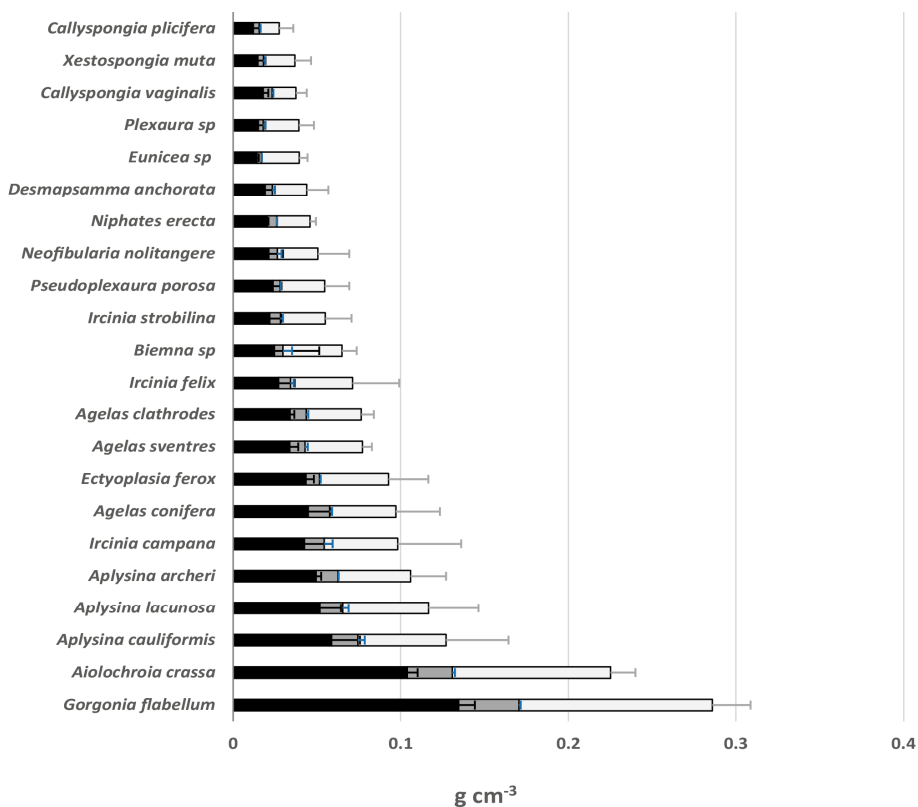


Figure S7. Proportions (mean \pm SE) of organic carbon (black bars), and organic nitrogen (grey bars), as well as absolute organic tissue (i.e., ash-free dry weight, whole bars) for erect reef organisms (i.e., massive sponges and gorgonians). $n = 3-4$ (see Table S1 for individual sample sizes). Raw data on biomass and elemental composition are provided in Online resource 2.

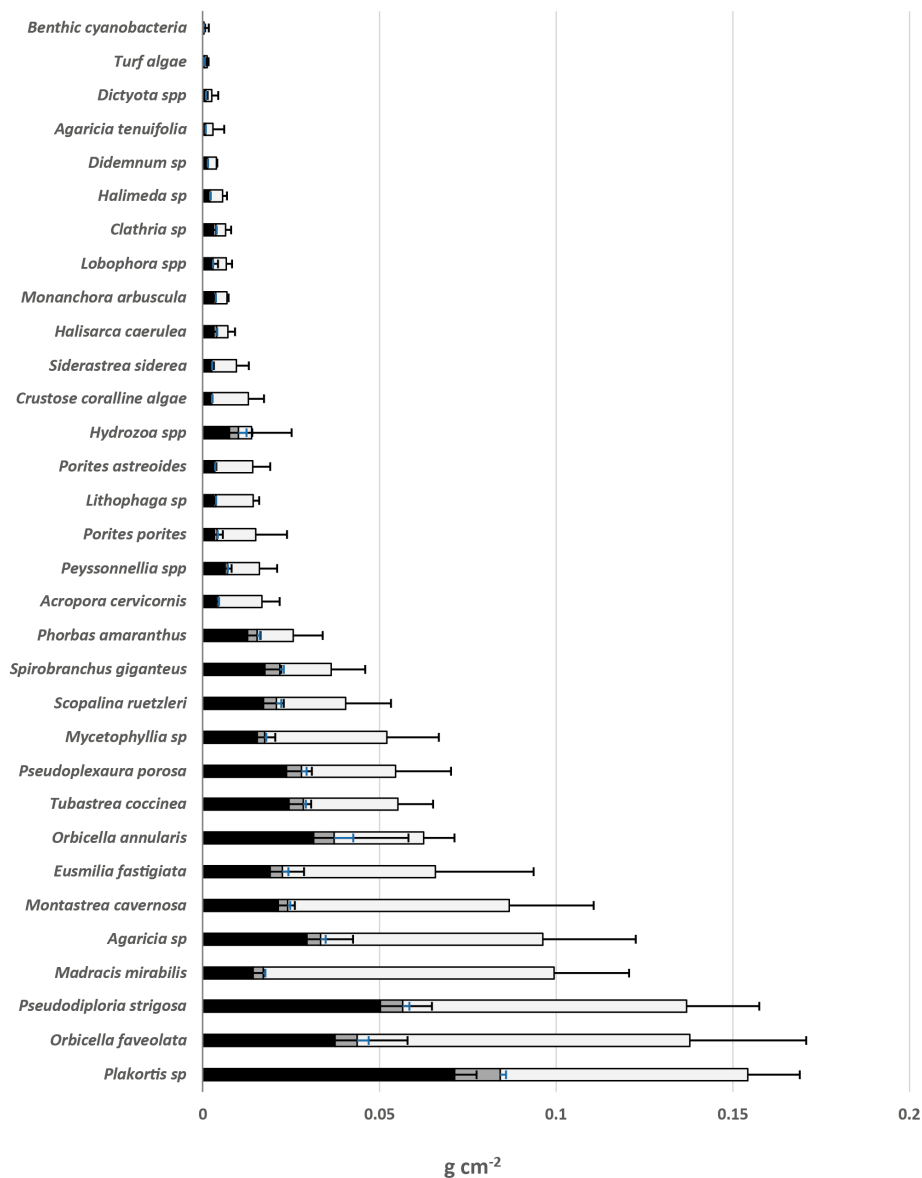


Figure S8. Proportions (mean \pm SE) of organic carbon (black bars), and organic nitrogen (grey bars), as well as absolute organic tissue (i.e., ash-free dry weight, whole bars) for non-erect reef organisms. $n = 3-9$ (see Table S2 for individual sample sizes). Corals were included in this category based on their morphological characteristics (i.e., thin layer of organic tissue on underlying inorganic skeleton). Raw data on biomass and elemental composition are provided in Online resource 2.

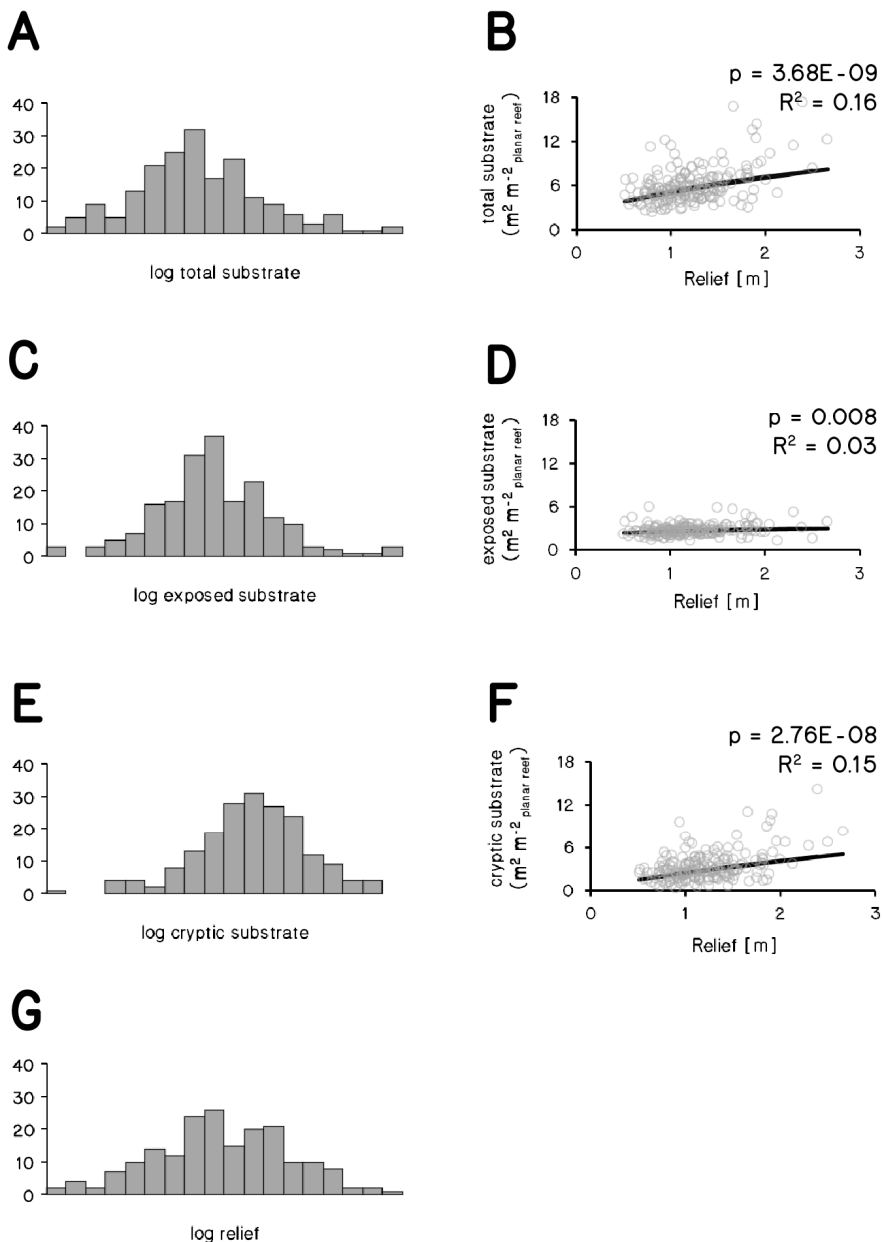


Figure S9. Histogram plots and linear regressions of total (**A, B**), exposed (**C, D**), and cryptic (**E, F**) substrate areas (in m^2 substrate area per m^2 projected reef) using relief as predictor variable (**G**). All data were log transformed to eliminate positive skew (**A, C, E, G**) and the resulting least squares predictions (black lines) were back-transformed before plotting (**B, D, F**). $n = 191$.

Supplementary tables

Table S1. Volume-normalized biomass (i.e., biomass per unit tissue volume, mean \pm SE) of erect reef organisms (i.e., gorgonians and massive sponges) in terms of ash-free dry weight and organic carbon in g per cm³.

organism	ash-free dry weight [g cm ⁻³]	organic carbon [g cm ⁻³]	n
gorgonians	0.113 \pm 0.032	0.051 \pm 0.015	14
<i>Eunicea sp.</i>	0.039 \pm 0.005	0.014 \pm 0.001	3
<i>Gorgonia flabellum</i>	0.286 \pm 0.033	0.135 \pm 0.014	4
<i>Plexaura sp.</i>	0.039 \pm 0.003	0.015 \pm 4.8E-04	4
<i>Pseudoplexaura porosa</i>	0.055 \pm 0.009	0.024 \pm 0.004	3
massive sponges	0.080 \pm 0.006	0.036 \pm 0.003	57
<i>Agelas clathrodes</i>	0.076 \pm 0.003	0.034 \pm 0.003	3
<i>Agelas conifera</i>	0.097 \pm 0.022	0.045 \pm 0.010	3
<i>Agelas sventres</i>	0.077 \pm 0.005	0.034 \pm 0.002	3
<i>Aiolochoiria crassa</i>	0.225 \pm 0.013	0.104 \pm 0.006	3
<i>Aplysina archeri</i>	0.106 \pm 0.015	0.050 \pm 0.006	4
<i>Aplysina cauliformis</i>	0.127 \pm 0.006	0.059 \pm 0.003	3
<i>Aplysina lacunosa</i>	0.117 \pm 0.022	0.052 \pm 0.010	3
<i>Biemna sp.</i>	0.065 \pm 0.011	0.025 \pm 0.004	3
<i>Callyspongia plicifera</i>	0.028 \pm 0.002	0.012 \pm 0.001	4
<i>Callyspongia vaginalis</i>	0.037 \pm 0.005	0.018 \pm 0.002	3
<i>Desmapsamma anchorata</i>	0.044 \pm 0.002	0.019 \pm 0.001	3
<i>Ectyoplasia ferox</i>	0.093 \pm 0.004	0.043 \pm 0.002	3
<i>Ircinia campana</i>	0.098 \pm 0.016	0.043 \pm 0.006	4
<i>Ircinia felix</i>	0.071 \pm 0.004	0.027 \pm 0.002	3
<i>Ircinia strobilina</i>	0.055 \pm 0.006	0.022 \pm 3.2E-04	3
<i>Neofibularia nolitangere</i>	0.051 \pm 0.005	0.021 \pm 0.002	3
<i>Niphates erecta</i>	0.046 \pm 0.011	0.020 \pm 0.005	3
<i>Xestospongia muta</i>	0.037 \pm 0.004	0.015 \pm 0.002	3

Table S2: Area-normalized biomass (i.e., biomass per unit tissue surface area, mean \pm SE) of all sampled organisms (except gorgonians and massive sponges) in terms of ash-free dry weight and organic carbon in g per cm². Superscripts on coral species indicate coral classification as massive corals (*), branching corals (+), encrusting corals (@), foliose corals (&), sheeting corals (\$), stalking corals (^), and solitary corals (^).

organism	ash-free dry weight [g cm ⁻²]	organic carbon [g cm ⁻²]	n
scleractinian corals	0.061 \pm 0.007	0.018 \pm 0.003	43
<i>Acropora cervicornis</i> ⁺	0.017 \pm 0.003	0.004 \pm 3.9E-04	4
<i>Agaricia agaricites</i> (sheeting) ^{@, \$}	0.096 \pm 0.015	0.030 \pm 0.008	3
<i>Agaricia agaricites</i> (foliose) ^{&}	0.015 \pm 0.002	0.002 \pm 2.7E-04	3
<i>Eusmilia fastigiata</i> ^{^^}	0.066 \pm 0.016	0.019 \pm 0.006	3
<i>Madracis mirabilis</i> ^{+, ^^}	0.099 \pm 0.012	0.014 \pm 0.002	3
<i>Montastrea cavernosa</i> [*]	0.087 \pm 0.014	0.021 \pm 0.003	3
<i>Mycetophyllia</i> sp. ^{@, \$}	0.052 \pm 0.008	0.016 \pm 0.003	3
<i>Orbicella annularis</i> [*]	0.063 \pm 0.005	0.031 \pm 0.015	3
<i>Orbicella faveolata</i> [*]	0.138 \pm 0.019	0.037 \pm 0.012	3
<i>Porites astreoides</i> [@]	0.014 \pm 0.003	0.003 \pm 4.7E-04	3
<i>Porites porites</i> ⁺	0.015 \pm 0.005	0.005 \pm 0.001	3
<i>Pseudodiploria strigosa</i> [*]	0.136 \pm 0.012	0.050 \pm 0.008	3
<i>Siderastrea siderea</i> [*]	0.010 \pm 0.002	0.002 \pm 0.001	3
<i>Tabastrea coccinea</i> [^]	0.055 \pm 0.006	0.024 \pm 0.004	3
encrusting sponges	0.042 \pm 0.013	0.019 \pm 0.006	21
<i>Clathria</i> sp.	0.006 \pm 0.001	0.003 \pm 4.6E-04	4
<i>Halisarca caerulea</i>	0.007 \pm 0.001	0.003 \pm 4.1E-04	4
<i>Monanchora arbuscula</i>	0.007 \pm 2.8E-04	0.003 \pm 2.1E-04	3
<i>Phorbas amaranthus</i>	0.026 \pm 0.005	0.013 \pm 0.002	3
<i>Plakortis</i> sp.	0.154 \pm 0.007	0.071 \pm 0.003	4
<i>Scopalina ruetzleri</i>	0.040 \pm 0.007	0.017 \pm 0.003	3
non-calcifying phototrophs	0.003 \pm 1.1E-04	0.001 \pm 5.2E-05	20
benthic cyanobacteria	0.00038 \pm 3.9E-05	1.6E-04 \pm 1.5E-05	8
<i>Dictyota</i> spp.	0.003 \pm 7.8E-05	0.001 \pm 2.5E-05	3
<i>Lobophora</i> spp.	0.007 \pm 5.7E-05	0.003 \pm 3.9E-05	3
turf algae	0.001 \pm 2.6E-05	0.001 \pm 1.7E-05	6
calcifying algae	0.012 \pm 0.002	0.003 \pm 0.001	10
crustose coralline algae	0.013 \pm 0.002	0.002 \pm 2.6E-04	4
<i>Halimeda</i> sp.	0.006 \pm 0.001	0.002 \pm 2.3E-04	3
<i>Peyssonellia</i> spp.	0.016 \pm 0.003	0.006 \pm 0.001	3
other	0.018 \pm 0.004	0.008 \pm 0.002	15
<i>Didemnum</i> sp.	0.004 \pm 1.7E-04	0.001 \pm 2.4E-04	3
<i>Hydrozoa</i> spp.	0.014 \pm 0.005	0.008 \pm 0.003	5
<i>Lithophaga</i> sp.	0.014 \pm 0.001	0.003 \pm 2.0E-04	3
<i>Spirobranchus giganteus</i>	0.036 \pm 0.005	0.018 \pm 0.002	4

Table S3. Illustration of geometrical approximations of massive sponge tissue volumes (similarly applied to gorgonians). Empty spaces of large oscula were also estimated and subtracted from total volume.

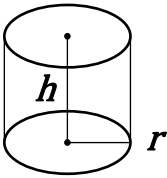

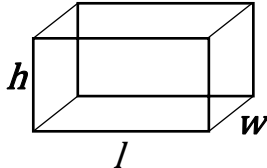

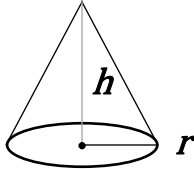
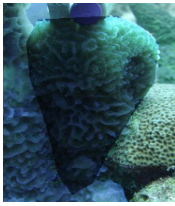
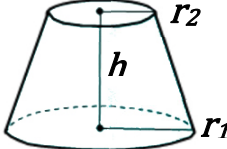

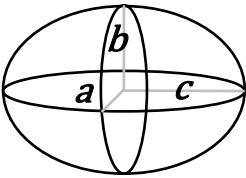

description	equation	geometrical shape	example
cylinder	$V = \pi r^2 h$		
rectangular prism	$V = l w h$		
cone	$V = \pi r^2 \frac{h}{3}$		
truncated cone	$V = \frac{1}{3} \pi (r_1^2 + r_1 r_2 + r_2^2) h$		
ellipsoid	$V = \frac{4}{3} \pi a b c$		

Table S4. Dimensions of algal tissue samples for estimating the relationship between canopy height and area-normalized biovolume. Canopy height for each sample was measured three times randomly across the sampled area and then averaged. Linear regression was performed on data grouped by canopy height (Figure S4A,B).

sample	planar area [m ²]	canopy height [m]	tissue surface area [m ²]	tissue volume [m ³]	biovolume [m ³ m ⁻²]
<i>Dictyota spp.</i>	0.008	0.004	0.007	2.9E-07	3.6E-05
<i>Dictyota spp.</i>	0.003	0.004	0.002	9.0E-08	3.6E-05
<i>Dictyota spp.</i>	0.003	0.005	0.003	1.1E-07	4.3E-05
<i>Dictyota spp.</i>	0.007	0.014	0.012	4.7E-07	6.5E-05
<i>Dictyota spp.</i>	0.003	0.038	0.004	1.8E-07	7.1E-05
<i>Dictyota spp.</i>	0.003	0.034	0.005	2.2E-07	8.7E-05
<i>Dictyota spp.</i>	0.008	0.052	0.025	9.9E-07	1.2E-04
<i>Dictyota spp.</i>	0.003	0.091	0.009	3.8E-07	1.5E-04
<i>Dictyota spp.</i>	0.003	0.083	0.010	4.1E-07	1.6E-04
<i>Lobophora spp.</i>	0.006	0.005	0.011	7.7E-07	1.2E-04
<i>Lobophora spp.</i>	0.003	0.003	0.005	3.6E-07	1.4E-04
<i>Lobophora spp.</i>	0.003	0.003	0.005	3.7E-07	1.5E-04
<i>Lobophora spp.</i>	0.016	0.010	0.028	2.0E-06	1.2E-04
<i>Lobophora spp.</i>	0.003	0.009	0.008	5.3E-07	2.1E-04
<i>Lobophora spp.</i>	0.003	0.010	0.007	4.8E-07	1.9E-04
<i>Lobophora spp.</i>	0.010	0.018	0.016	1.1E-06	1.1E-04
<i>Lobophora spp.</i>	0.003	0.021	0.007	4.9E-07	1.9E-04
<i>Lobophora spp.</i>	0.003	0.018	0.008	5.3E-07	2.1E-04

Supplementary data

This article contains supplementary data available at:

<https://doi.org/10.1007/s00338-021-02118-6>

Online resource 1. A docx file of the supplementary texts, figures, and tables shown in the previous sections.

Online resource 2. Volume- and biomass conversions. “Samples” lists raw results of the tissue analyses. Organisms are summarized in “summary” and different benthic groups are summarized in “communities”. Volume- and biomass standardizations for fleshy algae and subgroups thereof are based on their average canopy heights.

Online resource 3. Hidden cave surfaces and volumes. All surveyed quadrats are listed in rows, and columns show individual (hardly accessible and, thus, hand-measured) cavities in each quadrat. “hidden cavity surface areas” displays total surface areas and “hidden cavity volumes” displays cavity volumes, as approximated from simple geometrical shapes.

Online resource 4. Coral cryptic surface ratios. Proportion of cryptic surface in percent of live coral surface for individuals of sheeting and stalking corals.

Online resource 5. Percent cover. “horizontal percent cover” sheet lists raw results from horizontal (i.e., top-down) coral point counts. Sites are summarized in “horizontal site summaries” and communities are summarized in “horizontal communities”. The tab “horizontal cover incl layers” displays cover data that was used to calculate 3D metrics of reef communities (see Methods – “Relative cover on exposed and cryptic reef surfaces”). Percent cover and respective site summaries for percent cover on vertical and cryptic surfaces are provided in the following tabs.

Online resource 6. Absolute 3D surface cover. Surface areas of individual benthic biota for the total reef (reef summaries), as well as exposed areas (exposed summaries) and cryptic areas (cryptic summaries) individually. Communities are summarized in “communities”.

Online resource 7. Biovolumes and canopy heights. Canopy height measurements for individual surface types (horizontal, vertical, and cryptic) are listed in “canopy heights”, and summarized by site and surface type in “canopy summaries”. “emergent organisms” lists *in situ* measured biovolumes of massive sponges and gorgonians. Total volumes are summarized by site in “reef volumes” (total reef), “exposed volumes” (exposed reef), and “cryptic volumes” (cryptic reef). Benthic groups are summarized in “communities”.

Online resource 8. Standing stock of ash-free dry weights. Total weights are summarized by site in “reef summaries” (total reef), “exposed summaries” (exposed reef), and “cryptic summaries” (cryptic reef). Benthic groups are summarized in “communities”.

Online resource 9. Standing stock of organic carbon. Total weights are summarized by site in “reef summaries” (total reef), “exposed summaries” (exposed reef), and “cryptic summaries” (cryptic reef). Benthic groups are summarized in “communities”.

Online resource 10. Standing stock of organic nitrogen. Total weights are summarized by site in “reef summaries” (total reef), “exposed summaries” (exposed reef), and “cryptic summaries” (cryptic reef). Benthic groups are summarized in “communities”.

Online resource 11. Site coordinates and substrate surface areas. “substrates” sheet lists relief and surface areas of horizontal, vertical, and cryptic reef surfaces, as well as all surfaces combined (i.e., total surface area). Sites are summarized and coordinates are provided in “site summaries”.

Coral reef 3D reconstructions. 3D models of 191 m² of coral reef benthos are provided in an interactive format on Sketchfab (www.sketchfab.com) under the account “coralreefs.kornder”. Models are named by site and quadrat (e.g., Carmabi 1–16 chronologically relate to the 16 rows with site = Carmabi across all Online resources).

2

Additional supplementary data (see below) are available at figshare.com, along with the datasets listed above (DOI: 10.21942/uva.22592962). Additional requests regarding these resources should be directed to and will be fulfilled by the lead contact, Niklas A. Kornder (niklaskornder@gmail.com).

Raw images underlying digital 3D reconstructions. Images were obtained for each reconstruction using SCUBA, by circling around the area of interest while pointing a GoPro and three underwater video lights at the benthos. GoPro’s were set to time-lapse mode to acquire images in quick succession and generate sufficient overlap between consecutive images for the reconstruction (see Methods).

Raw images to estimate relative cover on different reef surfaces. Images of horizontal, vertical, and cryptic reef surfaces were analyzed in Coral Point Count with Excel extension (CPCe). One top-view image of each photo-quadrat was accompanied by three images of vertical and three images of cryptic reef surfaces within the reef framework underneath the quadrat (see Methods).

Coral Point Count report files. Files returned by CPCe, containing the locations and annotations of each point on the raw image analyses mentioned above.

Coral Point Count summaries. Summaries of the CPCe analyses per transect and meta-data in xlsx and csv format, including percent cover estimates and surface areas of the benthos depicted in the analyzed images.